Measurements of the Imbalance Response in a Rotor Supported on Tilting Pad Bearings and Integral Squeeze Film Dampers

by

Oscar De Santiago
Dr. Luis San Andrés

May 2000

TRC-SFD-1-00

Measurements of the Imbalance Response in a Rotor Supported on Tilting Pad Bearings and Integral Squeeze Film Dampers

EXECUTIVE SUMMARY

Measurements of the imbalance responses of a test rotor supported on a series tilting pad bearing and integral *SFDs* are described in detail. The rotor-bearing configuration is of interest in compressor applications where often oil lubricated dampers are introduced in series with fluid film bearings to relocate critical speeds, enhance the overall system damping, and reduce the risks of rotordynamic instabilities due to seals and impellers, for example.

Coast-down experiments from 10 krpm were conducted for increasing levels of disk imbalance. System damping coefficients are identified from the peak amplitude of rotor response (Q-factor) while traversing cylindrical mode critical speeds (~ 5,700 rpm for locked SFDs and ~3,000 rpm for active SFDs). The tests performed with locked (inactive) and active SFDs demonstrate the effectiveness of the flexible damped support in reducing the system critical speed and improving the overall rotor response with reduced transmitted forces to ground. The SFDs allow the rotor to operate safely with values of imbalance twice as large as the maximum sustained by the rotor supported on tilting pad bearings only.

The experiments continue to reveal a linear relationship between the peak amplitude of vibration at the critical speeds and the imbalance displacement, even for rotor motions larger than 50% of the tilting pad bearing and SFD clearances. In the most severe experiment, the largest imbalance induced dynamic loads up to five times the rotor weight. The tests also showed little cross-coupling effects with the shaft centerline moving along a nearly vertical path. The experimental results allowed benchmarking of TRC software for estimation of force coefficients in tilting pad bearings. Further experimental methods and procedures are needed to identify the force coefficients of the bearing support over desired frequency ranges.

ACKNOWLEDGEMENT

The additional support from NSF is gratefully acknowledged.

TABLE OF CONTENTS

LIST OF FIGURES

LIST OF FIGURES (CONTINUED)

LIST OF TABLES

NOMENCLATURE

c	Clearances for each type of element (bearing minimum radial clearance = 0.0762 mm, squeeze film damper radial clearance = 0.229 mm)
C_{crit}	System critical damping = $2(KM)^{1/2} = 2\xi M\omega_n$
Cij	Damping coefficients of tilting pad bearings, $i = X,Y$, $j = X,Y$
$C_{V,H}$	System damping coefficient in vertical and horizontal directions
H_{acc}	Amplitude of transfer function (Acceleration/load)
j	$\sqrt{-1}$
Kij	Stiffness coefficients of tilting pad bearings, $i = X,Y$, $j = X,Y$
$K_{V,H}$	System stiffness in vertical and horizontal directions
L	Length of each type of element (bearing = 22.9 mm, squeeze film damper = 23.0 mm)
m	Imbalance mass attached at rotor middle disk
M	Rotor mass (45.3 kg)
Q	Rotor-bearing system amplification factor
r	Radius of disk where imbalance mass is attached (114.3 mm)
r_{p_2}	Dimensionless journal bearing preload (0.405)
R^2	Linear regression correlation factor
u	Imbalance displacement (microns)
X,Y	Journal center coordinates, X: vertical, Y: horizontal
τ	Time constant of rotor-bearing system (257 sec)
$\omega_{nV,H}$	Natural frequencies in vertical and horizontal directions [rad/s]
ξ	System damping ratio

Subindexes

V,H	Vertical, horizontal (X,Y)
a	Denotes response on tilting pad bearings and locked dampers
b	Denotes response on tilting pad bearings and active dampers
c	Denotes response on ball bearings and active dampers

INTRODUCTION

Squeeze film dampers (*SFDs*) isolate components and dissipate energy from vibrating rotors in high-speed turbomachinery. A lubricant film fills the annular space between a stationary housing and a non-spinning journal free to follow precessional motions. A squirrel cage prevents the journal from rotation, provides stiffness to the damper support, and allows for tuning of the rotor-bearing system critical speeds away from the operation speed range. In most applications, a rolling element bearing connects the rotor to the damper journal. The Electro Discharge Machining (EDM) process allows the manufacturing of dampers with integral springs fit between the film arcuate lands. Integral *SFDs* offer the advantages of lower number of parts, shorter axial length, lighter weight, split manufacturing (which translate into easiness of installation), and higher tolerance precision. Experiments have also shown that end-sealed integral *SFDs* maintain adequate through flow rates which prevent lubricant overheating, and thus keep desired operating lubricant viscosities, unlike other types of conventionally sealed dampers (Dede et al, 1986, De Santiago and San Andrés, 1997).

Tilting Pad Journal Bearings (*TPJBs*) are widely used in turbomachinery to enhance rotordynamic performance by eliminating the source of fluid instability commonly associated with fixed geometry hydrodynamic bearings. The modern design of Flexure Pivot Tilting Pad Journal Bearings (*FPJBs*) offers similar performance as conventional *TPJBs*, with the additional advantage of an integral design which translates into simpler manufacturing, less number of parts, tighter tolerances and ease of installation.

The series combination of a tilting pad bearing and a squeeze film damper has been implemented in numerous compressors to introduce flexibility and damping to the bearing support (Zeidan, 1995). The proper design of these two mechanical elements allows for the optimum damping coefficient at the bearing support and accurate relocation of the (rigid mode) rotor bearing system critical speeds away from the operating speed range.

Measurements of imbalance responses of a test rotor supported on *SFDs* have been conducted since 1996. The experiments addressed rotor-*SFD* configurations typical of aircraft gas turbines where safety and stability dictate the use of ball bearings instead of

fluid film hydrodynamic bearings. The present report details the measurements of the synchronous imbalance response of a test rotor supported on flexure pivot, tilting pad bearings in series with integral *SFDs*. The major objectives of the experiments are to determine the combined effect of the hydrodynamic bearings and *SFDs* on the location of critical speeds and effective logarithmic decrement, and to demonstrate the effectiveness of this bearing pair combination on reducing amplitudes of rotor vibration. The experimental results also allow benchmarking of predictive computational tools for estimation of force coefficients in both tilting pad bearings and squeeze film dampers.

DESCRIPTION OF TEST RIG

Figure 1 depicts the drive motor and rotor supported on a pair of flexure pivot tilting pad bearings in series with integral squeeze film dampers. A 7.5 kW (10 HP) DC motor drives the rotor up to a top speed of 10,000 rpm through a flexible coupling and a drawn cup type roller clutch. Figure 2 shows the 43.5 kg (95.9 lb) rotor with a 76.2 mm (3 in) diameter shaft, 686 mm (27 in) long. The span distance between the support bearing centerlines is 406.4 mm (16 in). The three disks are 25.4 mm (1 in) thick and equally spaced from the rotor midspan. The drive end and middle disks are 279 mm (11 in) in diameter whereas the free end disk has a diameter of 229 mm (9 in). Each disk has 12 threaded holes, equally spaced on its circumference, for installation of calibrated imbalance masses. Hardened steel ring inserts provide the sliding surfaces at the fluid film bearing locations.

Two identical pedestals bolted to a metal base plate hold the test bearings and provide grooves for lubricant feeding into the damper lands, as well as drainage ducts for oil return. The pedestals have also transparent side covers allowing visualization of the bearing assembly. Custom-made plastic hose seals prevent leakage of lubricant to the pedestal's exterior while allowing free rotor lateral motions. A Delrin™ pin facing the rotor free end restricts rotor axial motions since no thrust bearings are installed in the test apparatus. The rotor, bearing pedestals and support steel plate rest on a steel-reinforced concrete table. A retractable steel cover provides protection and noise isolation, and an electrical blower also provides a stream of fresh air to cool the drive motor.

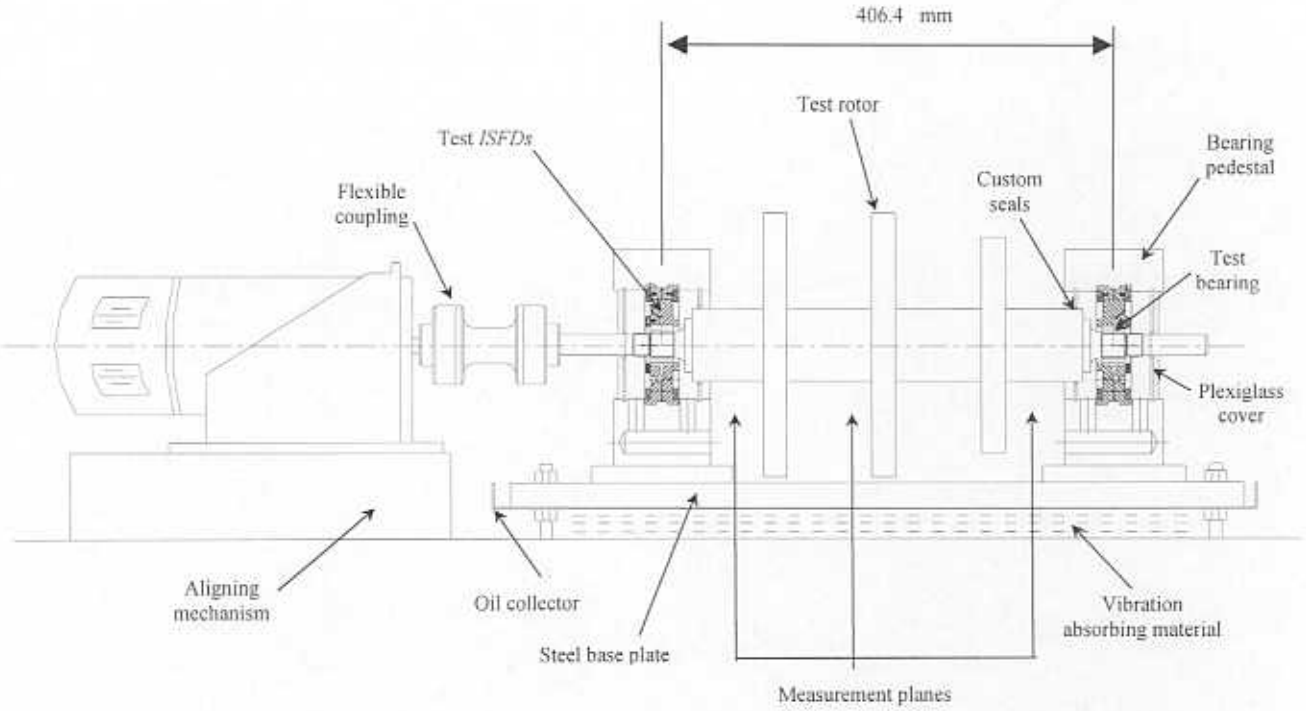

Figure 1. Test rig for measurements of imbalance response of rotor supported on tilting pad bearings and squeeze film dampers

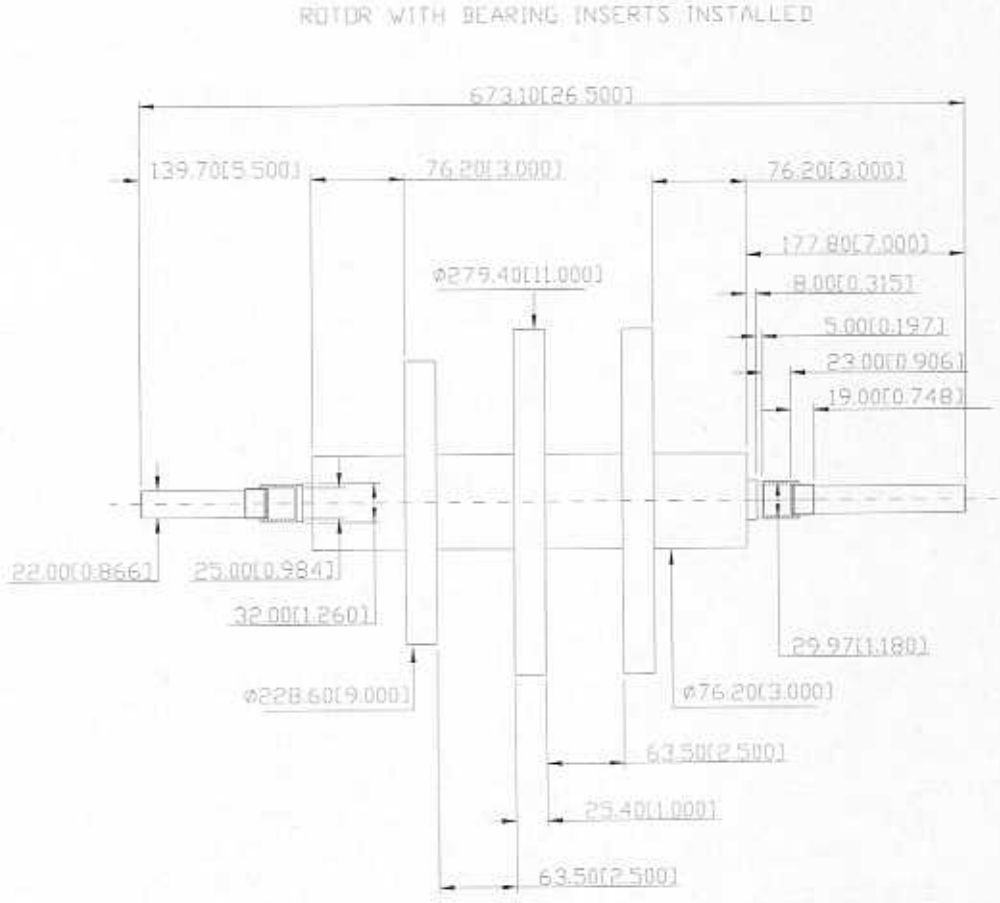

Figure 2. Geometry of three-disk rotor (weight 43.5 kg).

The experimental facility includes a 151 lt (40-gallon) lubricant reservoir with one main pump and a circulation system with a heater and a cooler to maintain the lubricant temperature at a desired pre-set value. The lubrication system, shown in Figure 3, provides oil to the tilting pad bearings and squeeze film dampers through separate lines and allows for independent control of the supply pressure to the bearing and damper elements.

Figure 4 depicts a schematic view of the instrumentation and sensors installed on the test rig. Eddy current proximity probes located at three axial planes and in two orthogonal directions measure the rotor vibration during coast down. Piezoelectric accelerometers with magnetic bases record the pedestals vibrations. The Bentley Nevada ADRE® data acquisition system records the rotor response and supports acceleration as functions of the rotor speed and stores the data in a personal computer. Type K thermocouples and meters display reservoir, inlet and exit lubricant temperatures from the test bearings as well as ambient temperature for reference, and the motor temperature for safe operation. A signal conditioner and three oscilloscopes display rotor orbits in the planes of measurement and a two-channel frequency analyzer shows the vibration spectrum components in real time. A light beam optical tachometer displays the rotor speed and provides a reference signal to the data acquisition system for phase angles measurement.

Turbine type digital flow meters show the overall and individual lubricant consumption of the test bearings and dampers, and gauges display the lubricant supply pressure into each bearing and damper. The lubricant employed in all tests is ISO VG 10 turbine oil. Table 1 presents the measured lubricant viscosity as a function of temperature.

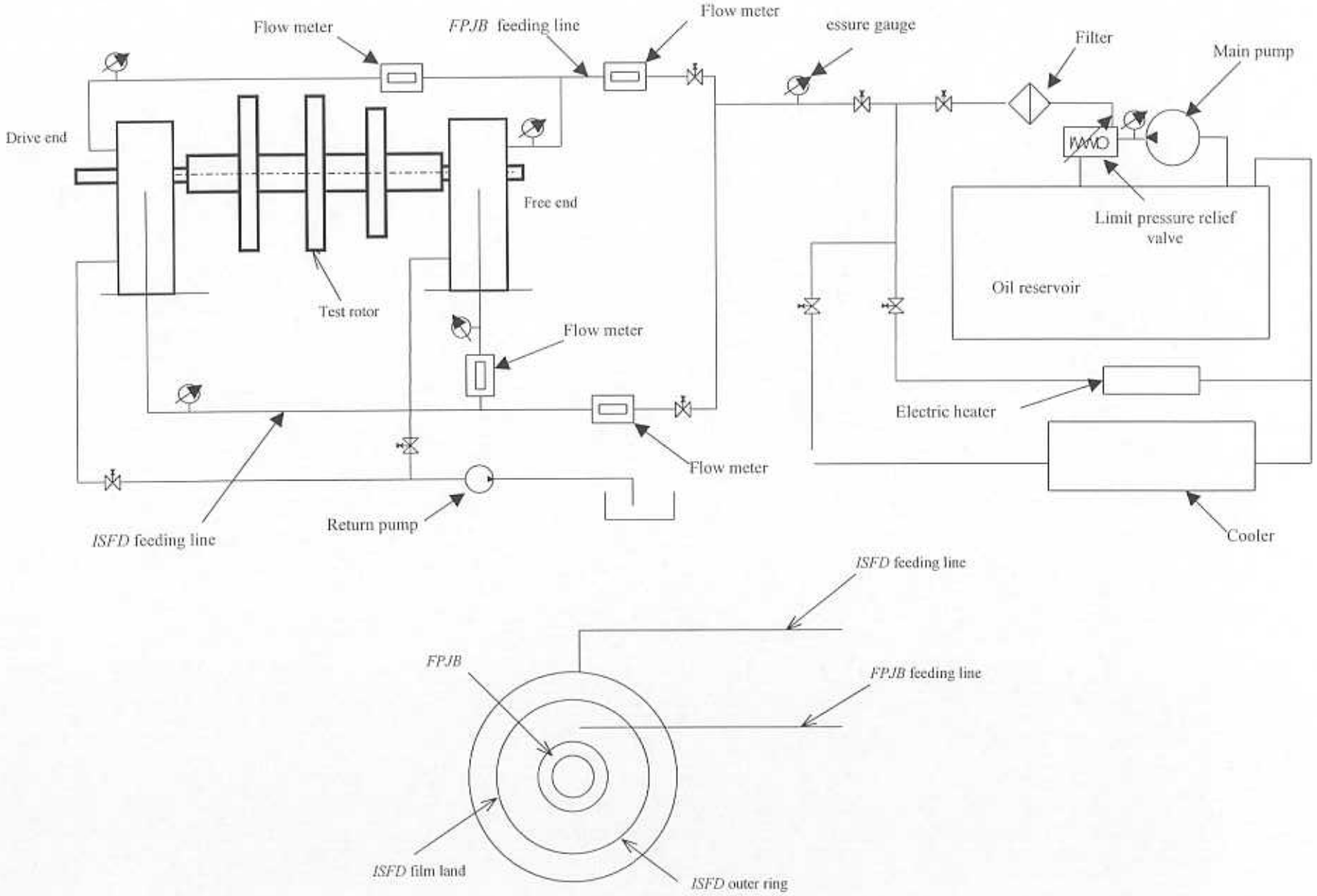

Figure 3. Lubrication system for tilting pad bearings and squeeze film dampers.

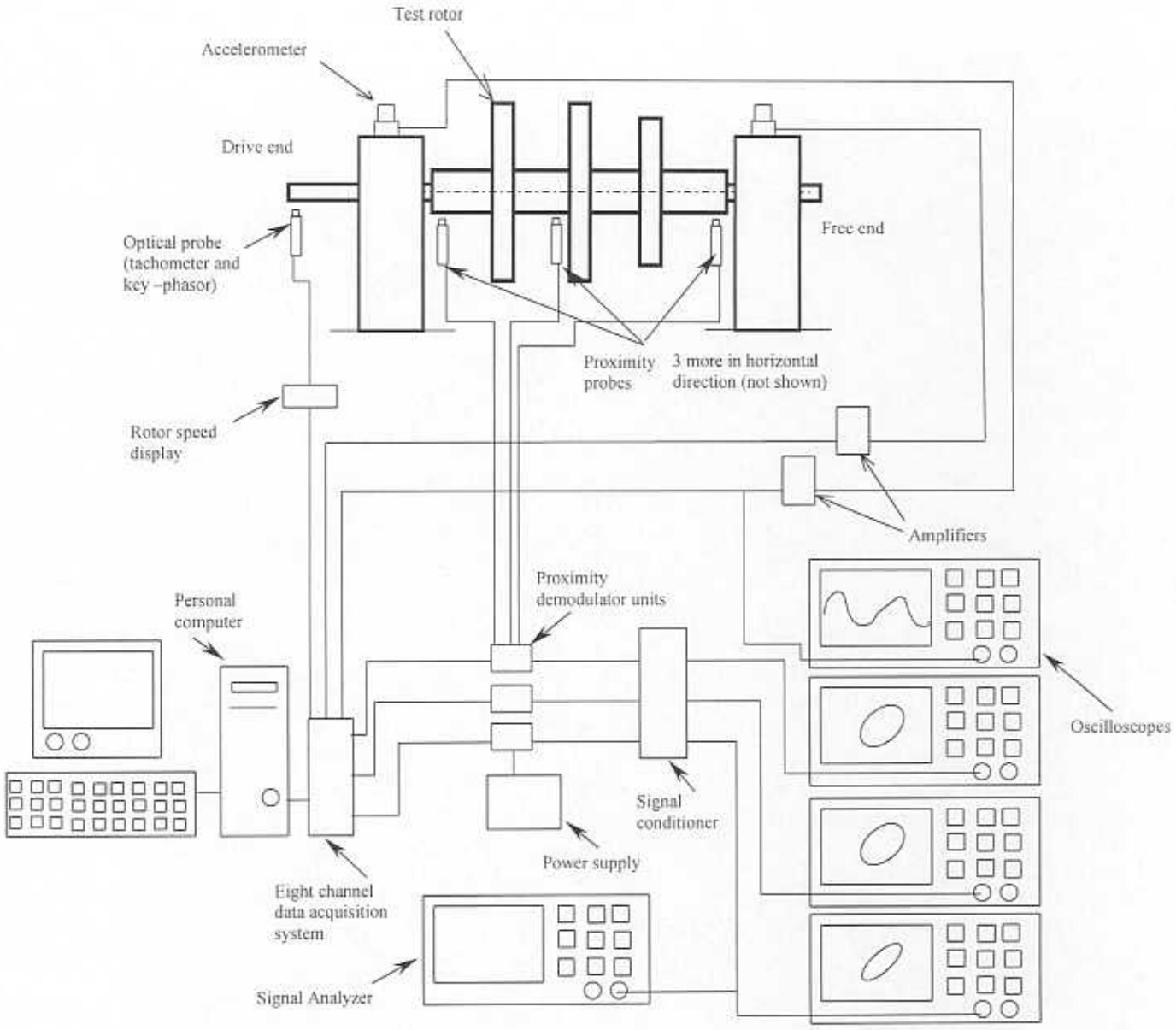

Figure 4. Instrumentation for rotor imbalance response measurements.

DESCRIPTION OF INTEGRAL DAMPERS AND TILTING PAD BEARINGS

Figure 5 shows the test integral squeeze film damper consisting of an outer ring, 126 mm (4.961 in) in outer diameter with a circumferential groove for lubricant supply, and an inner ring (damper journal) on which a tilting pad bearing fits. Four pairs of EDM S-shaped springs connect the outer and inner rings as shown in the detail portrayed in Figure 6. A small clearance of 0.229 mm (9 mils) separates the two rings into four film lands (pads) where hydrodynamic pressure generates the damping forces. The clearance around the damper journal is manufactured uneven so that the journal becomes centered under the springs' deflection due to the shaft weight. The damper film lands have an arc extent of 52°, axial length of 23 mm (0.906 in) mm and a radius of 48.15 mm (1.90 in). The inner ring originally accommodating ball bearings, was modified to hold a tilting pad bearing.

The outer ring has four 1.6 mm (0.063 in) diameter holes that serve as inlet lubricant ports to the squeeze film lands from the external groove. The inner ring has a lateral feeding port and an internal groove for oil supply into the tilting pad bearing. A flexible hose connection provides the lubricant to the tilting pad bearing through the damper journal from an independent supply line.

De Santiago and San Andrés (1999) detail the design procedure for the flexure pivot tilting pad journal bearings (*FPJBs*) to render the optimum support damping when combined with the current integral dampers. Figure 7 shows a schematic view of the *FPJB* and Table 2 describes its main characteristics. The babbitt-lined tilting pad bearing has four pads, 70° in extent, with the rotor static load directed between pad pivots. The bearing nominal diameter is 45.97 mm (1.181 in), and the bearing assembled (minimum) radial clearance is 0.076 mm (3 mils) with a dimensionless preload (r_p) of 0.405. The pivot circumferential offset is 0.55. The bearing pads are lubricated through injection ports connected to the supply groove.

Figure 8 shows the combined support *ISFD-FPJB* as installed in the test rig. Note that the bearing support has two fluid films acting in series. Furthermore, the tilting pad bearings develop a hydrodynamic film and reaction forces only when the rotor spins.

Recall that the dynamic properties (stiffness and damping) of a *FPBJ* depend both on the rotor speed and the frequency of vibration (Childs, 1993).

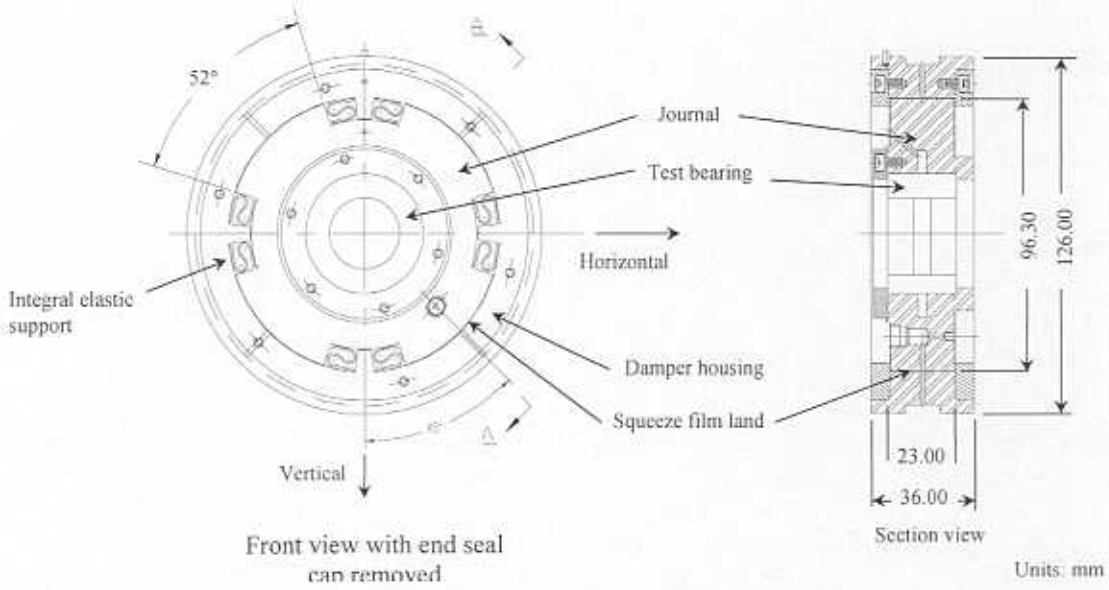

Figure 5. Test integral squeeze film damper.

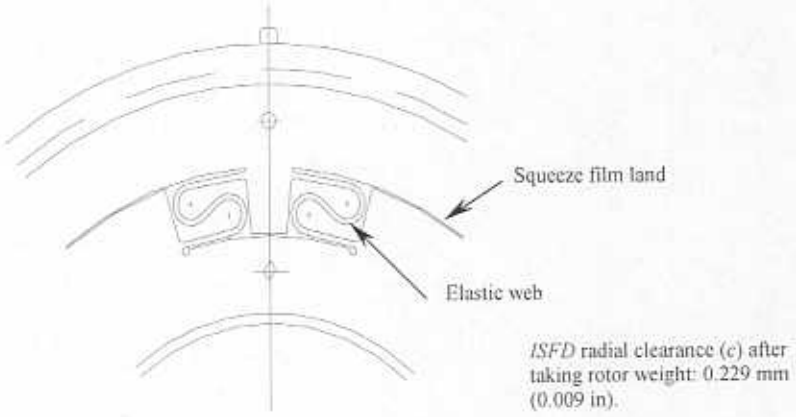

Figure 6. Detail of structural webs on integral damper.

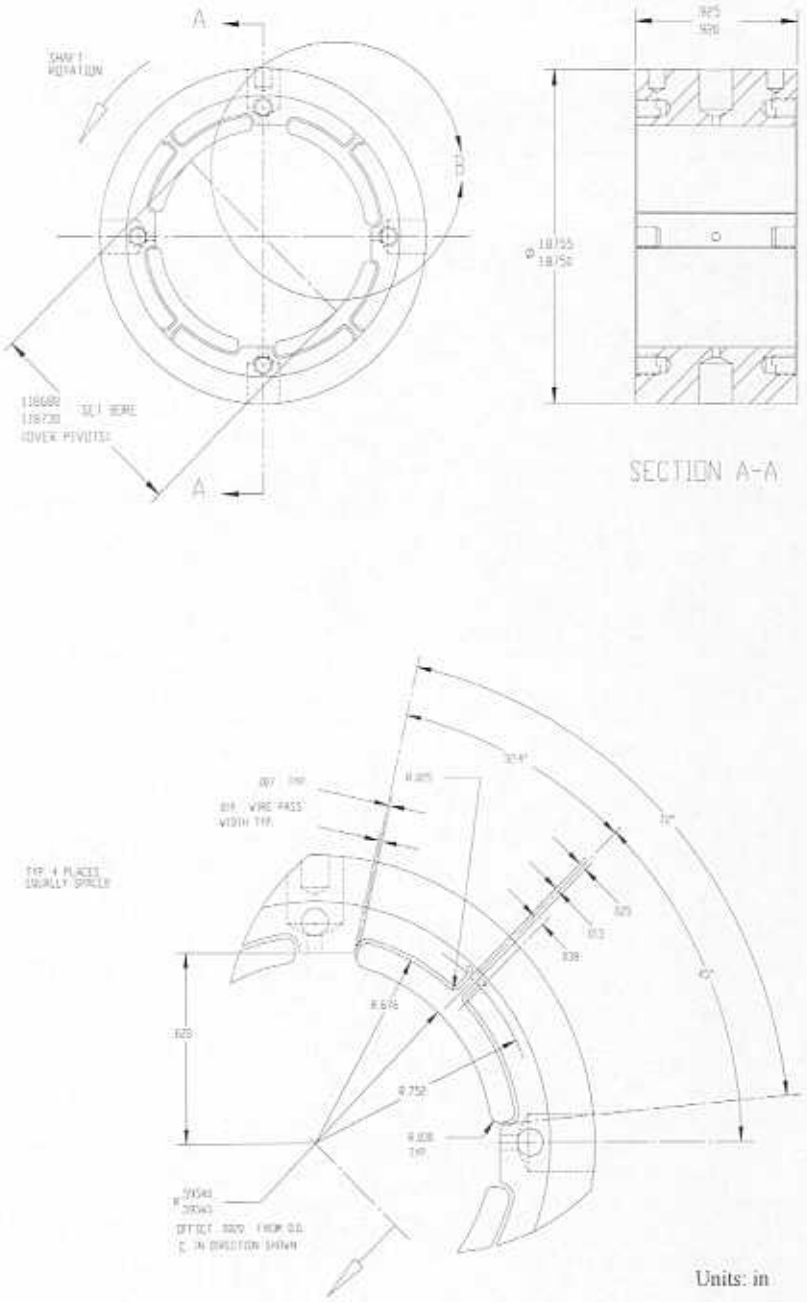

Figure 7. Dimensions of flexure pivot tilting pad journal bearing.

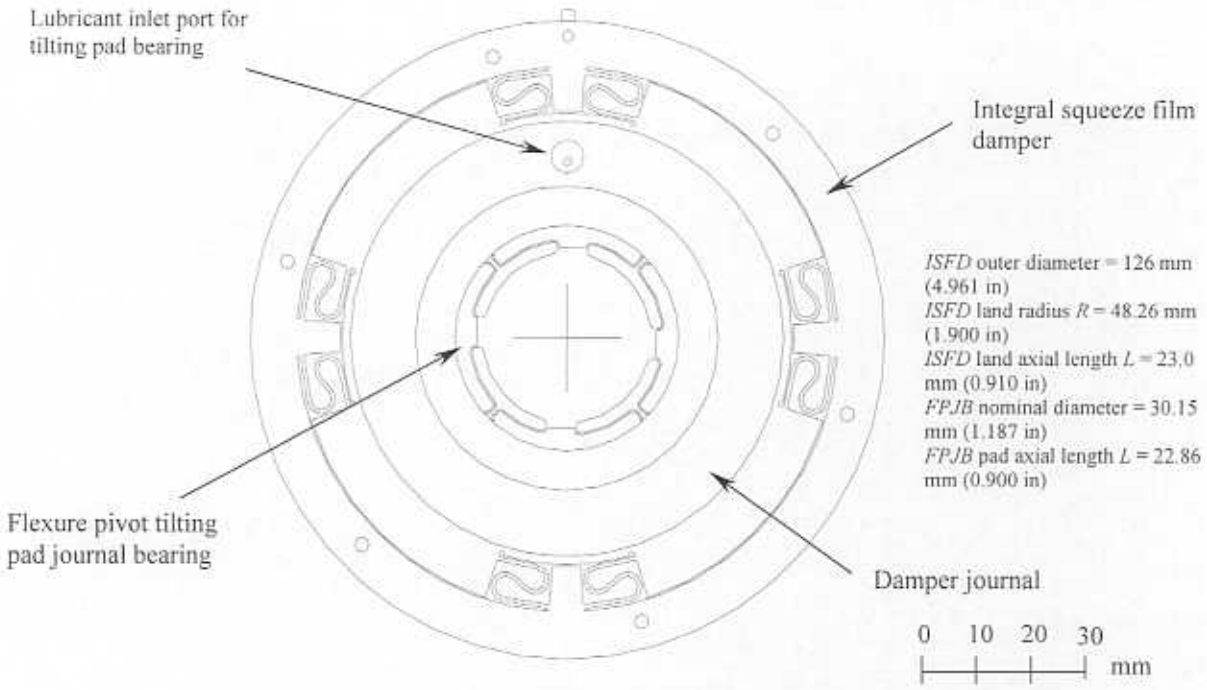

Figure 8. Assembled ISFD and tilting pad bearing.

EXPERIMENTAL RESULTS

Lubricant flow rates through bearings

Figure 9 shows the measured flow rates versus the external pressure supply for both integral dampers and the two flexure pivot tilting pad bearings. The measurements, conducted at a lubricant temperature equal to 70°F, (21.1°C), show the flow rates are proportional to the supply pressure; and with less flow through the *FPJBs* due to their smaller clearance and reduced film land area. Adequate flow to the tilting pad bearings operating at the highest speed of 10,000 rpm is insured for supply pressures above 0.90 bars (13.5 psig).

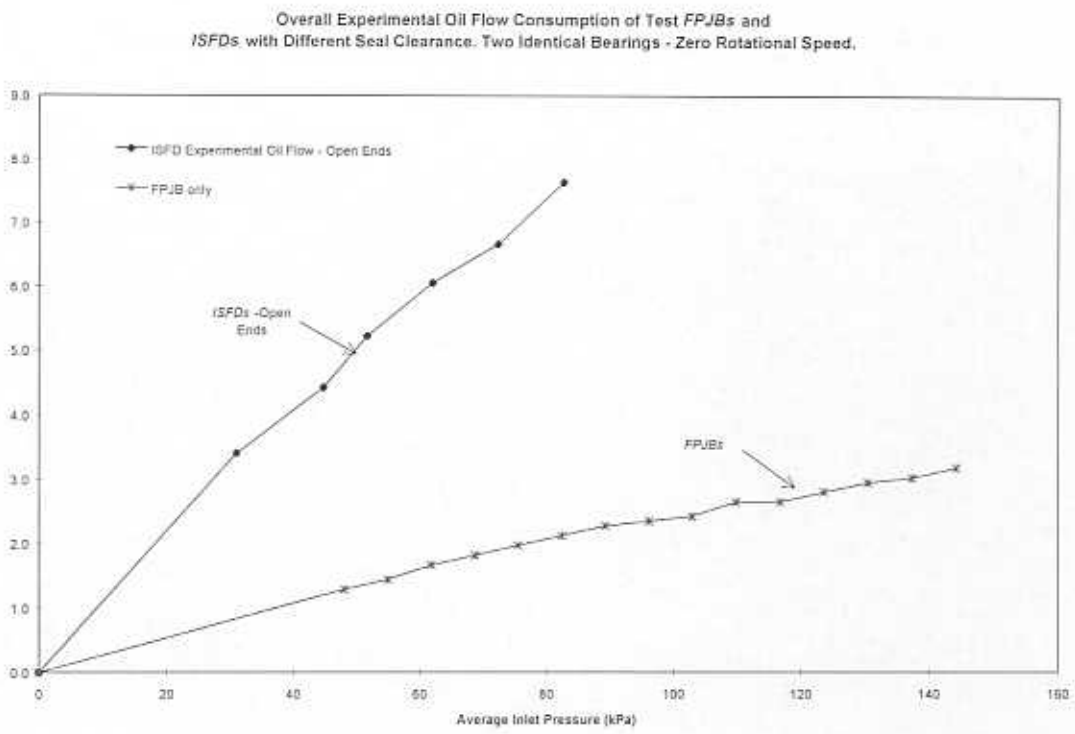

Figure 9. Flow rates for both integral dampers and two tilting pad bearings.

Preliminary response tests with no rotor imbalance

A preliminary test with no imbalance in the rotor evidences the rotor lift within the bearing clearances. Figure 10 shows in dimensionless form the centerline travel of the rotor at the drive and free ends for increasing rotational speeds. The *FPJB* minimum diametrical clearance (0.152 mm, 6 mils) is used to set dimensionless rotor displacements. The main direction of the shaft centerline motion is along a vertical line thus denoting small cross-coupled forces. The coordinate (0,0) denotes the beginning of the test with the rotor at its lowest position and in contact with the pads. At the highest speed of ~10,000 rpm, the rotor has lifted to about 20% of the bearing clearance.

Note that the rotor center does not return to the same start position, thus revealing some static sag at the end of the experiment. This may be attributed to the bearing construction, the data acquisition system accuracy, and some thermal induced bow of the rotor.

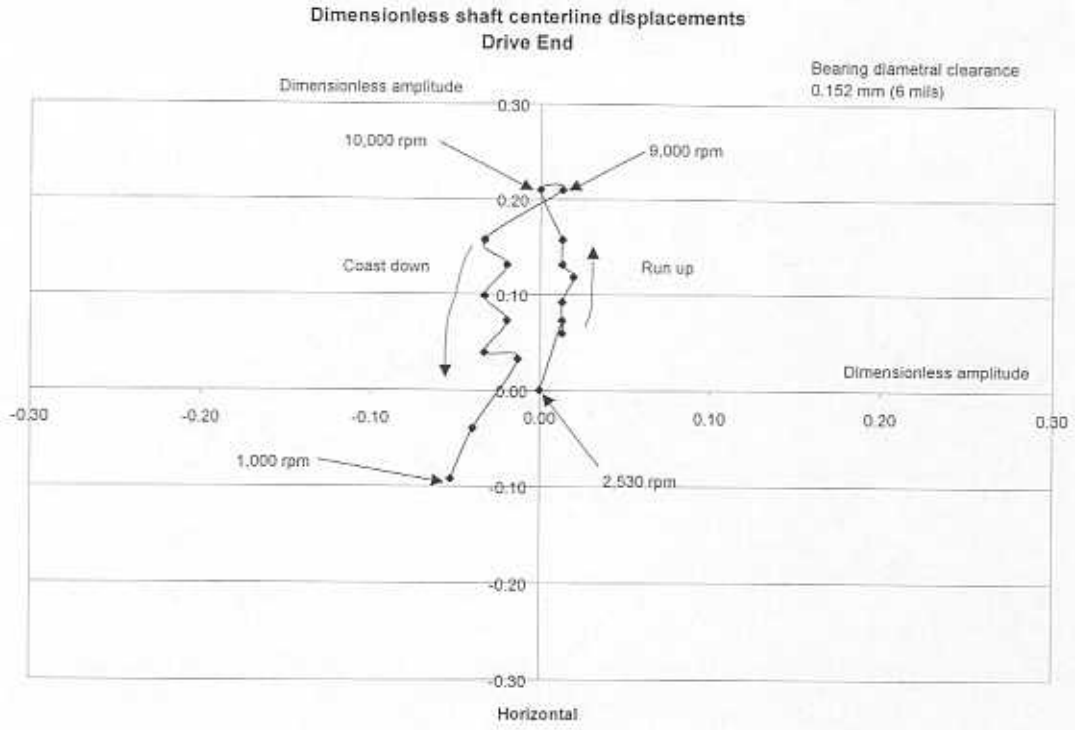

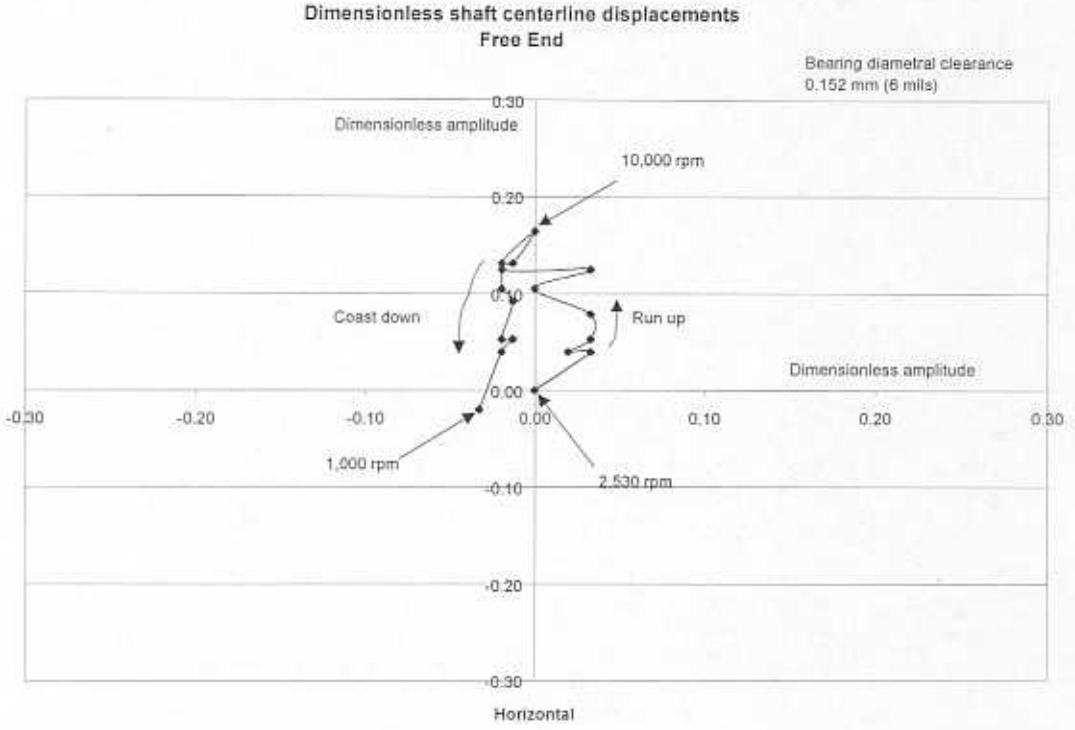

Figure 10. Shaft centerline motion for test with no imbalance. Rotor supported on *FPJBs* in series with *ISFDs*.

Figure 11 shows the rotor deceleration curves for a typical coast down test with no imbalance. The figure compares the decay in speed and time constants (τ) for the rotor supported on ball bearings and *ISFDs* (De Santiago and San Andrés, 1998) and the current rotor supported on the series *FPJBs* and integral dampers. The time constants for both conditions are 226 s and 257 s, respectively. The experimental results evidence the very low friction in the *FPJBs* and the long time, above 10 minutes, required for the rotor to come to a full stop.

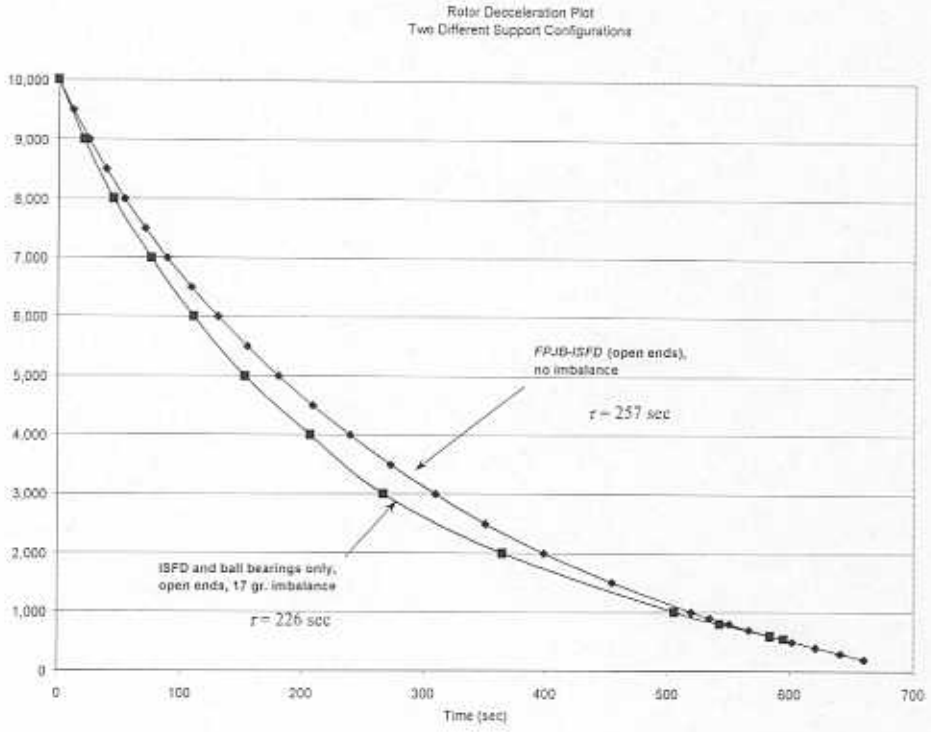

Figure 11. Comparison of deceleration curves for rotor supported on ball bearings-*ISFDs* and series *FPJB-ISFDs*.

System damping coefficients from impact response tests

Impact response experiments were performed on the rotor supported on the series *FPJB-ISFDs* at null rotational speed to re-assess the damping capability of the open-ended integral dampers. A calibrated impact hammer strikes the rotor middle disk (very close to the rotor cg) in the vertical and horizontal directions, and a piezoelectric accelerometer attached on the opposite side of the disk records the ensuing rotor motion. Figure 12 shows typical (vertical and horizontal) rotor accelerations versus time, averaged transfer functions (acceleration/load) and coherences from averaging thirty impact responses. The amplitude of the transfer function (H_{acc}) at the resonance peak and the natural frequency (ω_n) renders the system damping coefficient, i.e.

$$C = \left| \frac{\omega_n}{jH_{acc}(\omega_n)} \right| \qquad (1)$$

The estimation of the system damping assumes the rotor is a rigid point mass supported on two parallel identical supports. These assumptions have been repeatedly verified throughout the research program since 1996. Note that the fundamental natural frequencies for the rotor supported on the *FPJB-ISFDs* are equal to 57 Hz and 52 Hz in the vertical and horizontal directions, respectively.

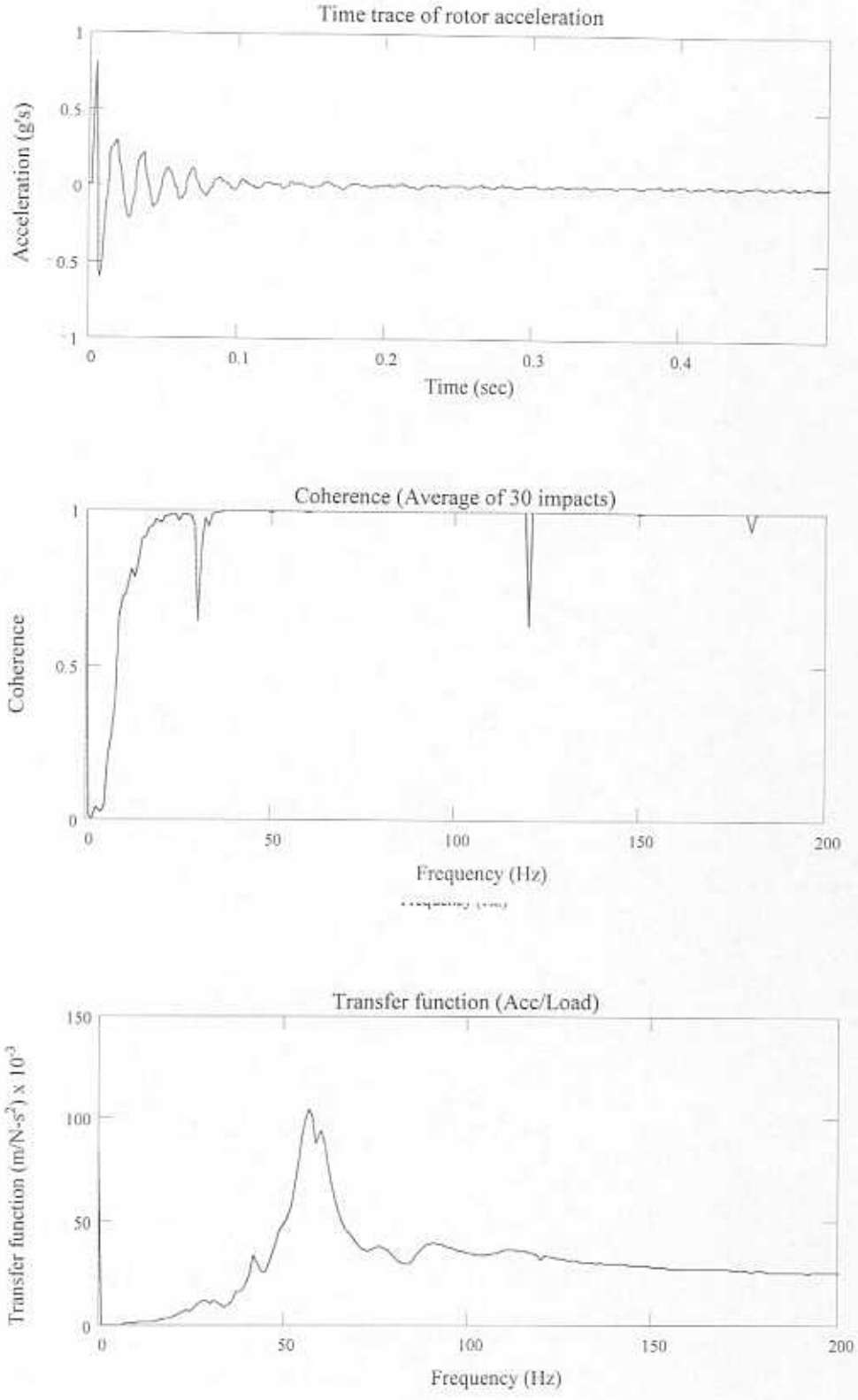

Figure 12a. Rotor response to impacts supported on series *FPJB-ISFDs*. Null rotor speed. Vertical direction, lubricant temperature T = 90.5°F (32.5°C).

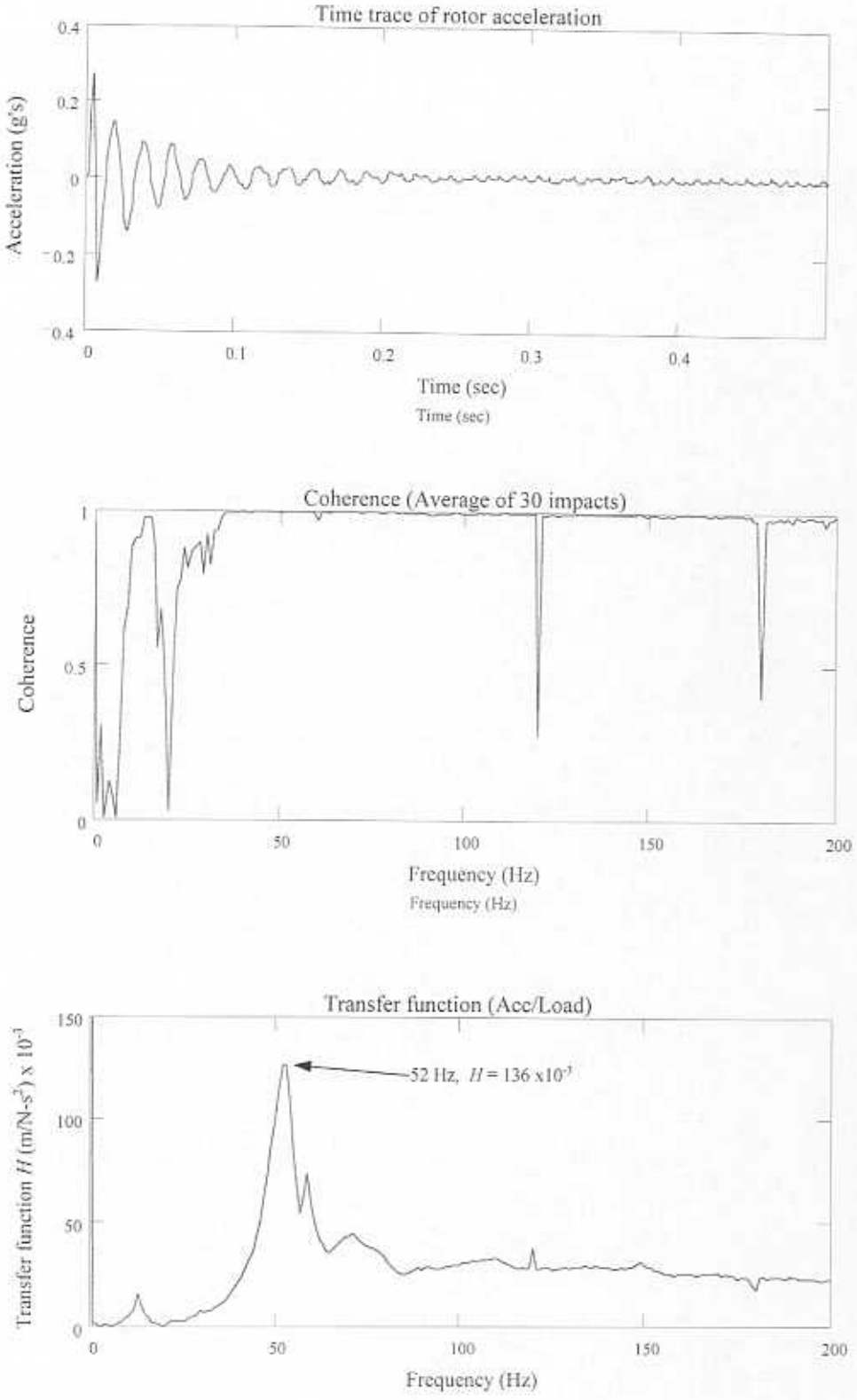

Figure 12b. Rotor response to impacts supported on series *FPJB-ISFDs*. Null rotor speed. Horizontal direction, lubricant temperature T = 77°F (25°C).

Figure 13 shows the identified system damping coefficients from the impact load tests for increasing lubricant viscosities (temperatures). Note that the current system yields larger values of the system damping coefficient (11% average increase in the horizontal direction, and 18% in the vertical direction) as compared with the rotor supported on open ended *ISFDs* only (De Santiago and San Andrés, 1998). The reason for the increment in damping may be due to the lubricant entrapped in the small clearance behind the pads of the flexure pivot tilting pad bearings. A slight increment of 1 Hz in the natural frequencies was recorded when comparing to the natural frequencies of the test rotor supported on ball bearings and *ISFDs*.

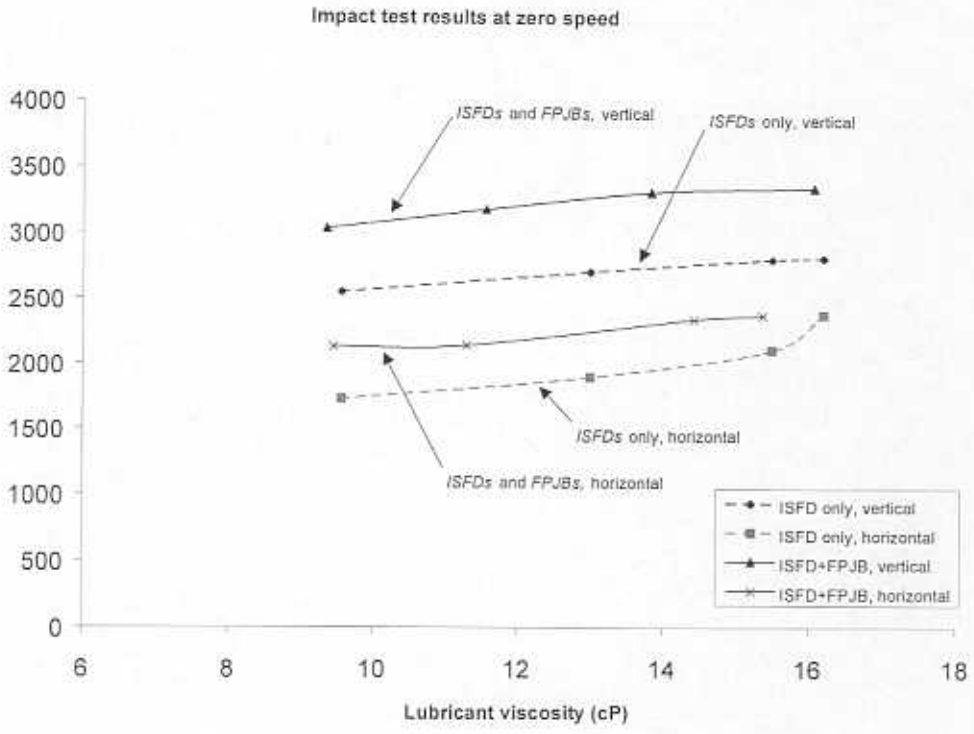

Figure 13. System damping coefficients vs. lubricant viscosity as estimated from impact tests. Rotor supported on series *FPJB-ISFDs*. Comparison are shown with results of similar tests for rotor supported on *ISFDs* only (open ends).

Results of imbalance response for rotor supported on tilting pad bearings only

The current bearing support configuration allows conducting measurements with the integral dampers locked. These experiments are of importance to isolate the effect of the tilting pad bearings on the dynamic response of the rotor. Bronze shims inserted within the integral damper film lands and lateral plates tightly pressed against the damper journal and housing ring effectively eliminated (locked) any damper journal motions relative to its housing.

In all the synchronous response measurements that follow, the baseline response to remnant imbalance is subtracted vectorially from the responses due to known imbalance masses inserted at a radius of 114.3 mm (4.5 in) on the rotor middle disk and exciting the first (cylindrical) mode of vibration.

Table 3 sums the imbalance conditions and inlet lubricant temperatures. The largest imbalance displacement *(u)* corresponds to 22.4 microns, i.e. approximately 30% of the *FPJB* assembled radial clearance. Figure 14 depicts the compensated rotor synchronous response at midspan for increasing imbalances. Similar measurements were recorded at the free and drive ends and not shown for brevity. Note that the amplitude of rotor vibration in the vertical direction is consistently larger than in the horizontal direction. In fact, the horizontal rotor response does not show a clear critical speed peak within the test speed range.

Table 4 shows the peak-peak amplitudes of response at the first critical speed in the vertical direction as well as the location of the critical speeds. Figure 15 shows the average amplitude response versus the imbalance distance (*u*). The standard deviation of the averaged amplitudes in the three planes of measurement provides an estimation of the scattering of the amplitude data. Note that the largest imbalance (u = 22.4 microns) excites rotor motions up to ~80% of the assembled bearing clearance at the drive end location. A linear regression fit to the peak average response shows a correlation factor R^2 equal to 0.86.

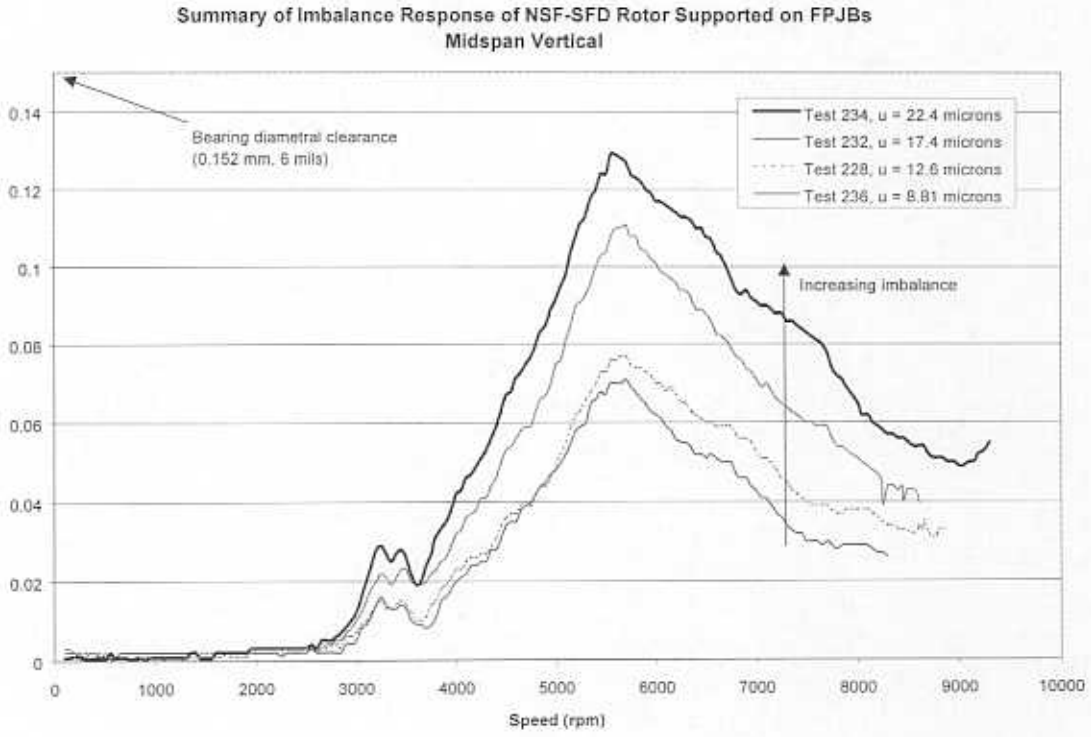

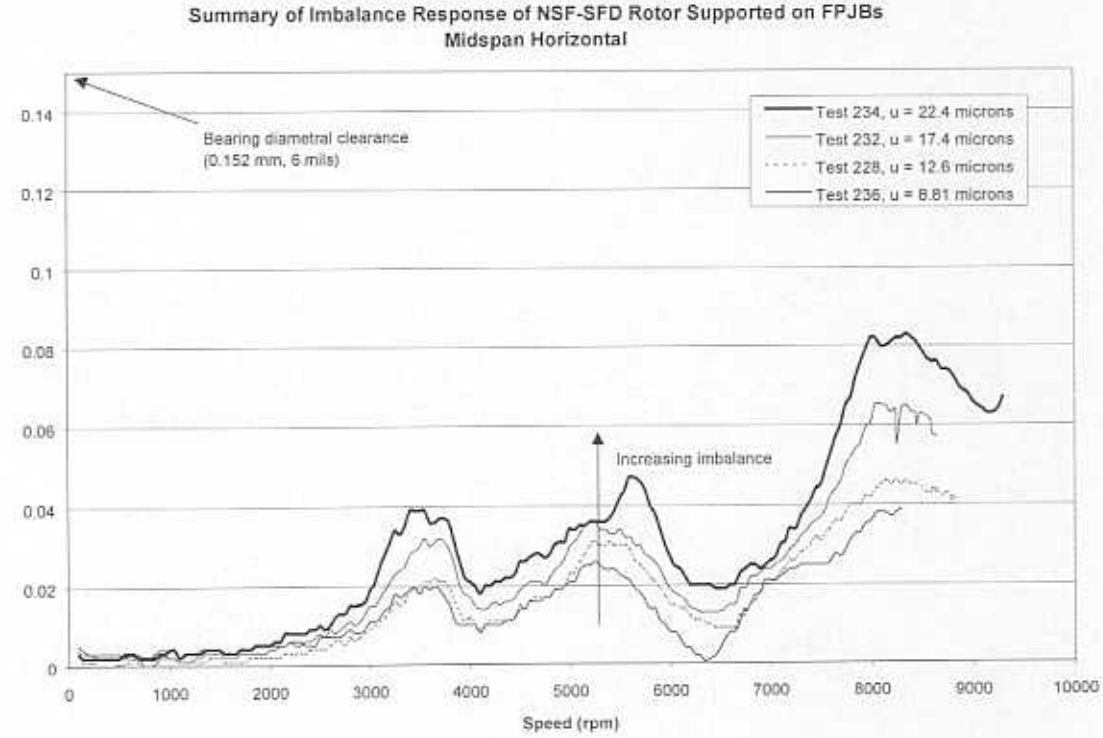

Figure 14. Imbalance response of rotor supported on *FPJBs*. Measurement at rotor midspan (vertical and horizontal). Locked *ISFDs*.

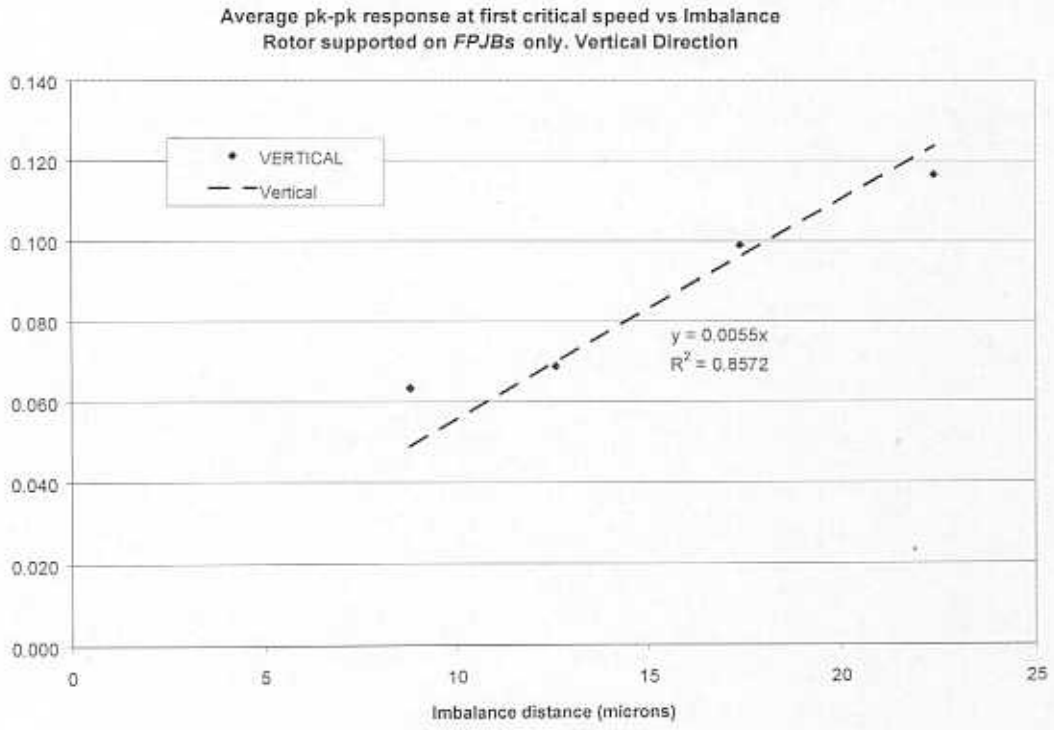

Figure 15. Average peak-peak rotor response at first critical speed versus imbalance distance for rotor supported on *FPJBs*. Vertical direction. Critical speed ~5750 rpm.

Figure 16 shows dimensionless amplitudes of rotor response recorded at midspan for two different levels of imbalance (u). The corresponding imbalance (u) is used to obtain the dimensionless response. The measurements show the linearity of the response, i.e. proportional to the imbalance displacement, even though the amplitudes of motion are rather large relative to the bearing clearance.

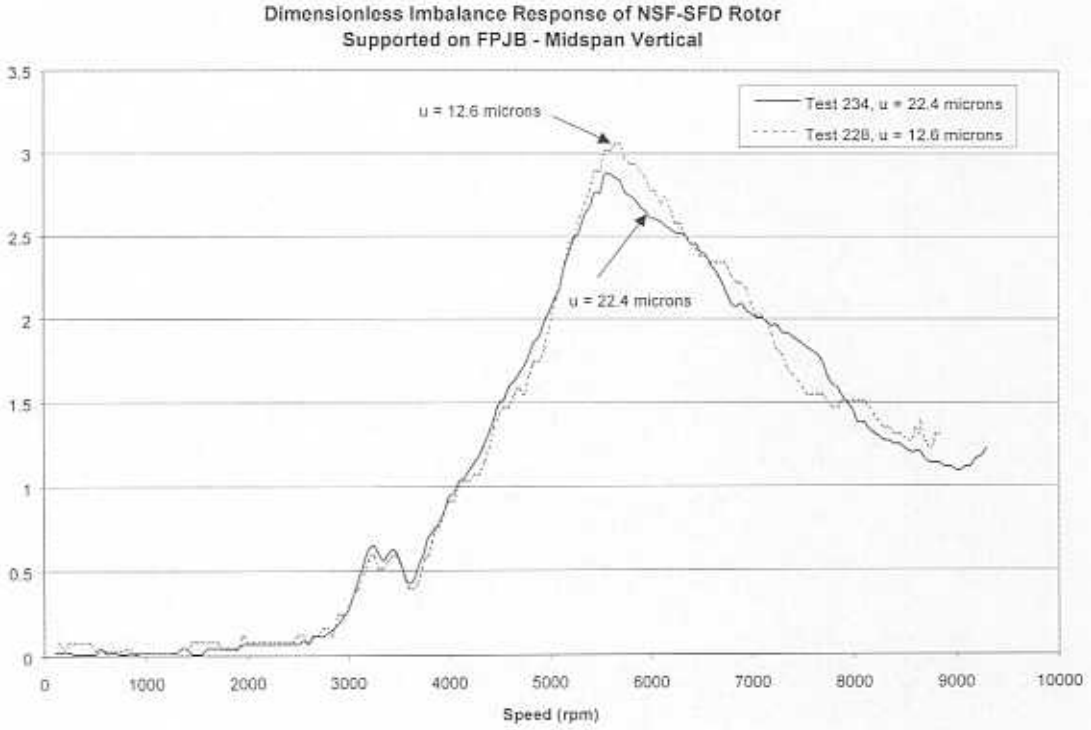

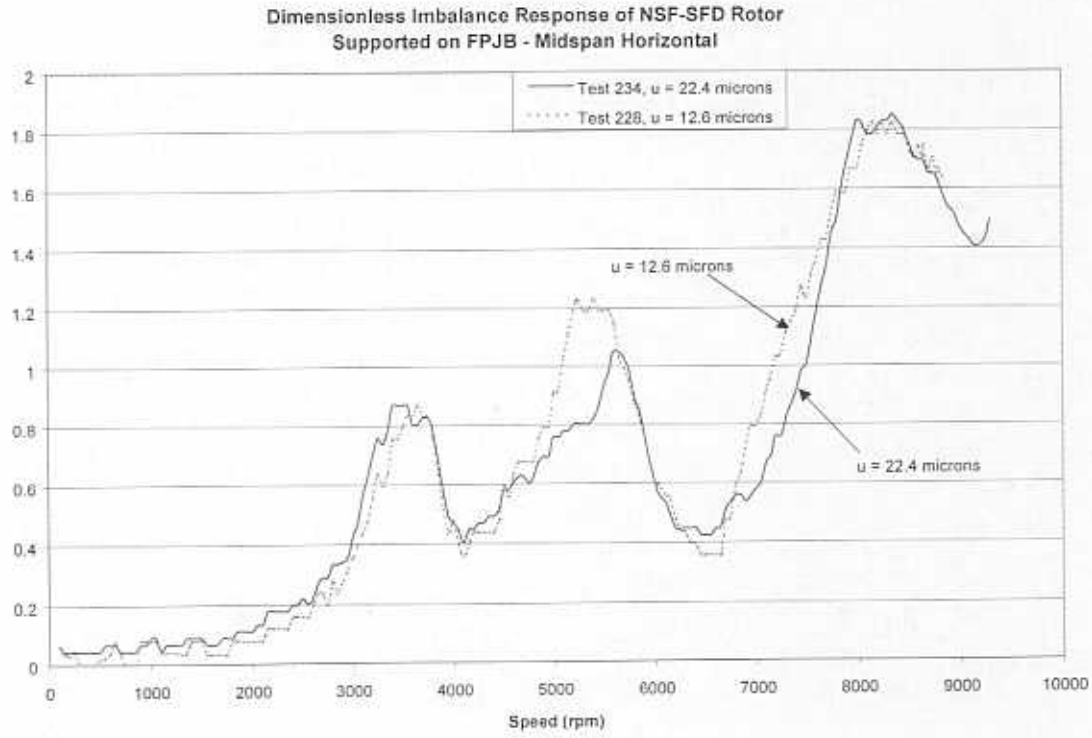

Figure 16. Dimensionless imbalance response of rotor supported on *FPJBs* only. Measurement at midspan.

An experiment was conducted to verify that the damper journal was effectively locked. A miniature accelerometer attached to the free end *ISFD* journal recorded its vibration in the vertical direction, and an additional accelerometer attached to the bearing pedestal provided a reference signal for the housing absolute motion, as shown in Figure 17. Figure 18 depicts the acceleration amplitude versus rotor speed for both sensors in a test with a 5-gram imbalance. Note that both signals are nearly identical, thus demonstrating that the damper journal was effectively locked.

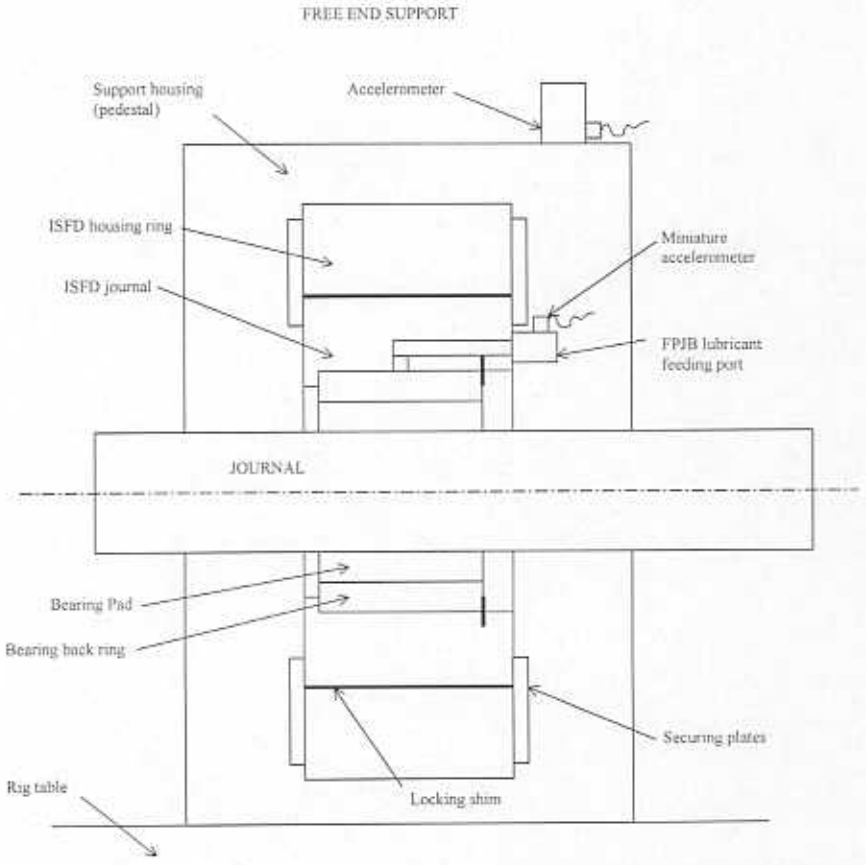

Figure 17. Location of accelerometers on locked *ISFD* (journal) and bearing support.

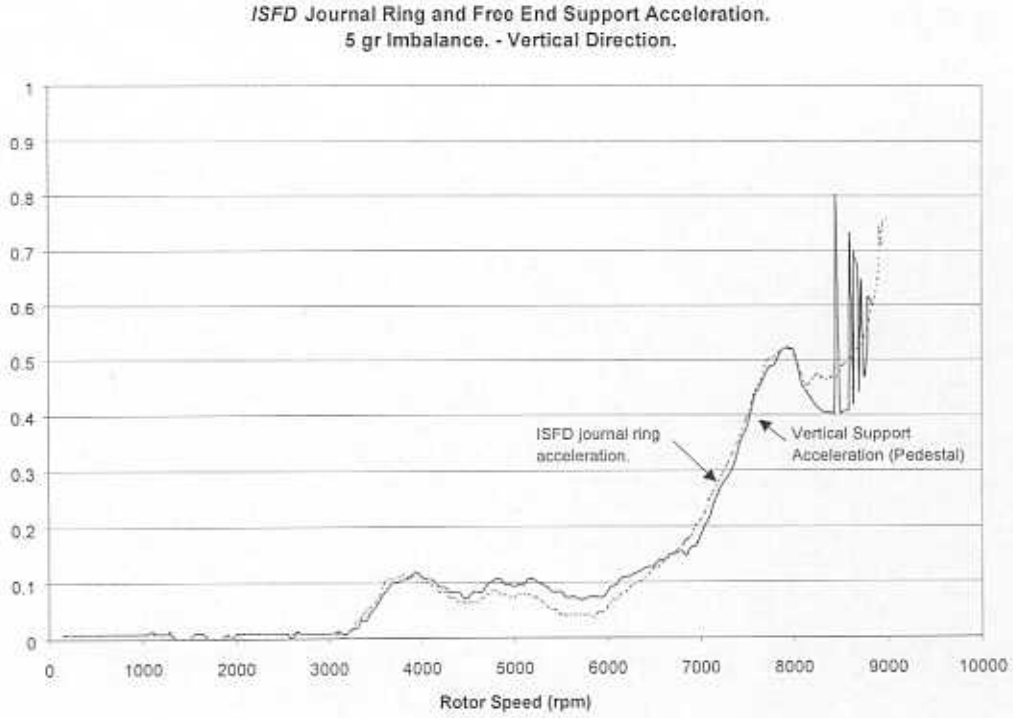

Figure 18. Comparison of accelerations for locked damper journal and bearing pedestal (vertical direction, imbalance= 5 gram).

Figure 19 shows the dimensionless shaft centerline travel (relative to the *FPJB* assembled clearance) at the drive and free end supports for the largest imbalance of 8.9 grams. Note that the static travel of the shaft is nearly vertical, thus showing little cross-coupled forces. The shaft centerline motion at the top speed reaches about 50% of the bearing assembled clearance. The test with the largest imbalance shows a small subsynchronous vibration component at a rotor speed of 6,800 rpm. Figure 20 shows the vibration spectrum with an incipient subsynchronous component at 0.49 times the running speed, i.e. 56 Hz, which corresponds with the natural frequency of the rotor supported on the series *FBJB-ISFDs*, although the dampers were apparently locked (see Figure 18). This test was the only one where subsynchronous activity became apparent. Incidentally, the subsynchronous component remained stationary for the short range of speeds (less than 500 rpm) in which it appeared.

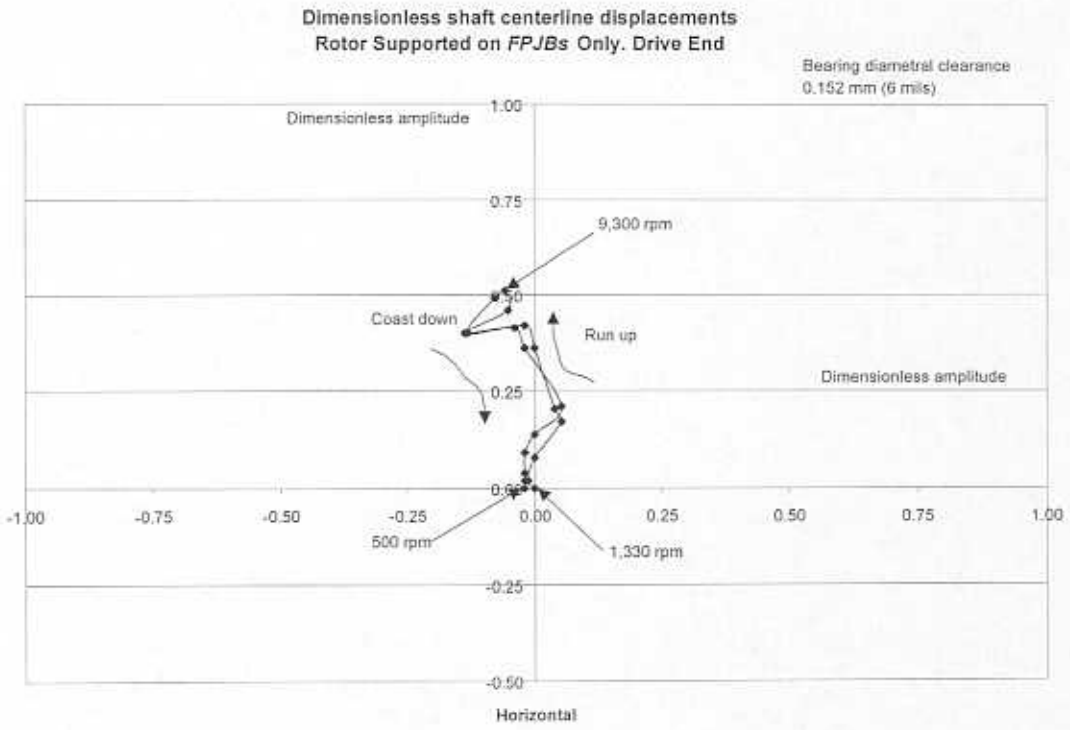

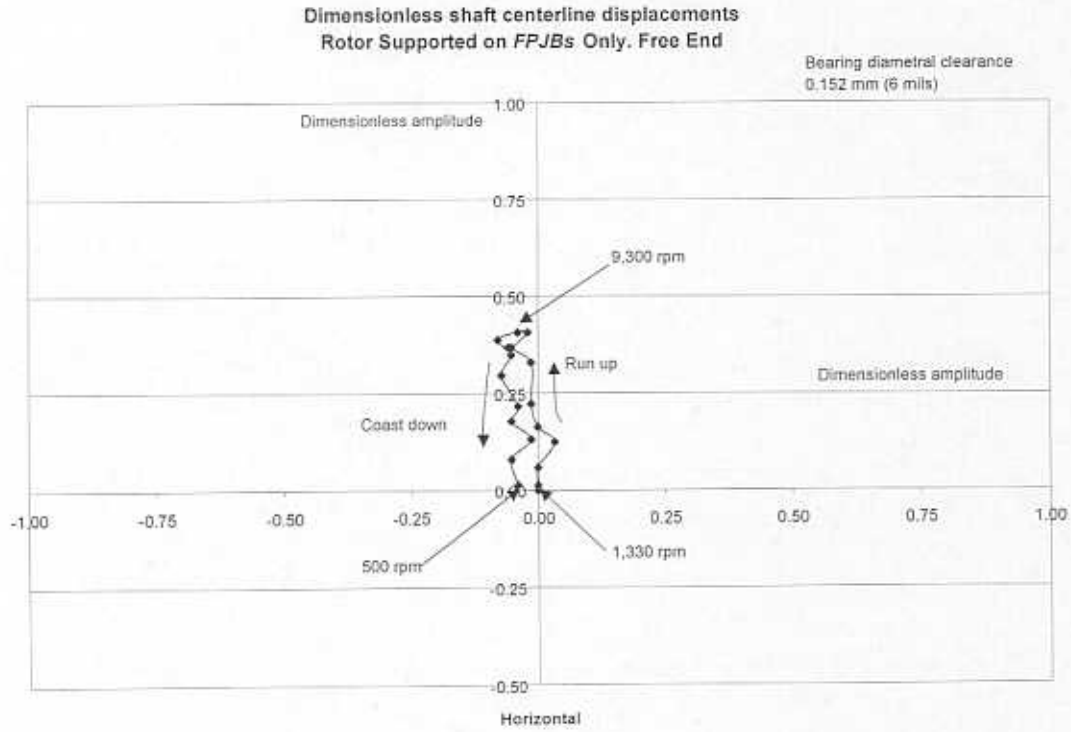

Figure 19. Shaft centerline motion at drive and free end supports for imbalance 8.9 grams (u=22.4 microns) Rotor supported on *FPJBs* only

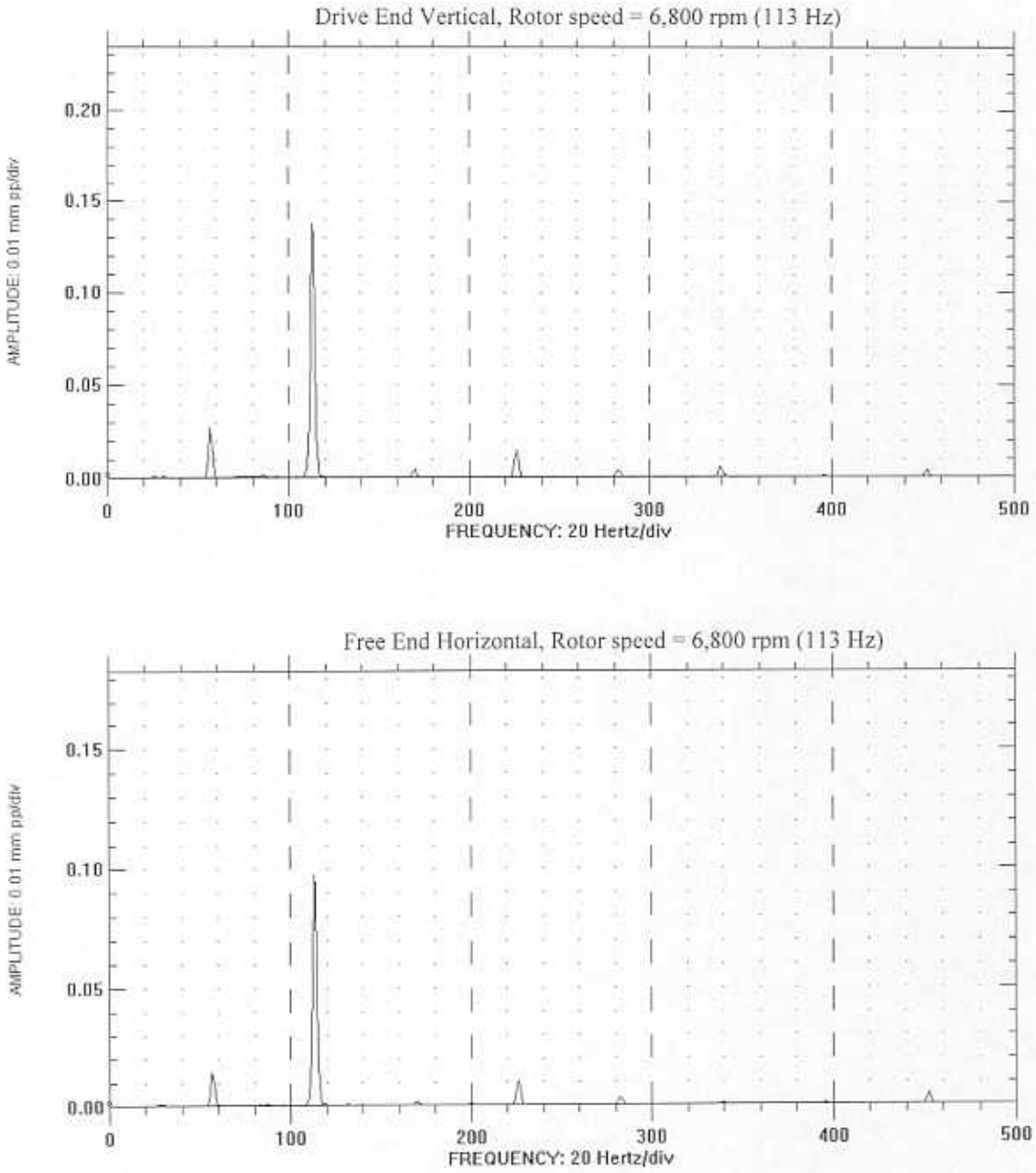

Figure 20. Spectrum of rotor vibration at 6,800 rpm during coast down. (8.9 gram imbalance). Rotor supported on *FPJBs* only. Drive and free end supports.

Predictions of imbalance response for rotor supported on tilting pad bearings only

A 38 stations transfer matrix model implemented into the calculation program *XLRotor* © predicts the synchronous rotor response to imbalance. Table 5 shows a favorable comparison of the model predictions and the measured free-free natural frequencies for the rotor. The experimental measurements are derived from impact tests. Note the large influence of the coupling on the first elastic natural mode of vibration.

The computational program *HydroTRCM* © (San Andrés, 1996) is used to estimate the synchronous stiffness and damping force coefficients of the tilting pad bearings for the noted static loads and operating conditions given in Table 2. Figure 21 depicts the calculated rotordynamic coefficients as functions of the rotor speed. Note that both bearings show similar stiffness and damping values in the two orthogonal directions (X: vertical, Y: horizontal), although the drive end bearing has larger coefficients as a result of its larger static load. The small cross-coupled stiffnesses maintain the same sign along the speed range, and thus do not favor the onset of hydrodynamic film induced instability.

The bearing pedestals are known to be quite flexible, and their effect must be taken into account for accurate prediction of the rotor dynamic response (De Santiago et al, 1997). Table 6 provides the stiffness magnitudes for the integral dampers and the bearing pedestals as estimated from impact tests in the vertical and horizontal directions. The equivalent values correspond to the series combination of the integral dampers and pedestal stiffnesses.

Figures 22 shows the predicted stiffness and damping force coefficients resulting from the combination of the *FBJB* synchronous force coefficients and the pedestal stiffnesses. Note that the combined support shows remarkable differences in stiffness as compared to the *FPJB* alone due to the flexibility of the supports. Also note that the stiffness coefficients become more uniform in the range of speeds.

Table 7 presents predictions of the system critical speeds and damping ratios for rotor speeds below 10,000 rpm. All predicted modes of vibration are well damped within the range of test speeds. In the experiments, the imbalance masses located on the middle disk effectively excite the cylindrical mode of vibration.

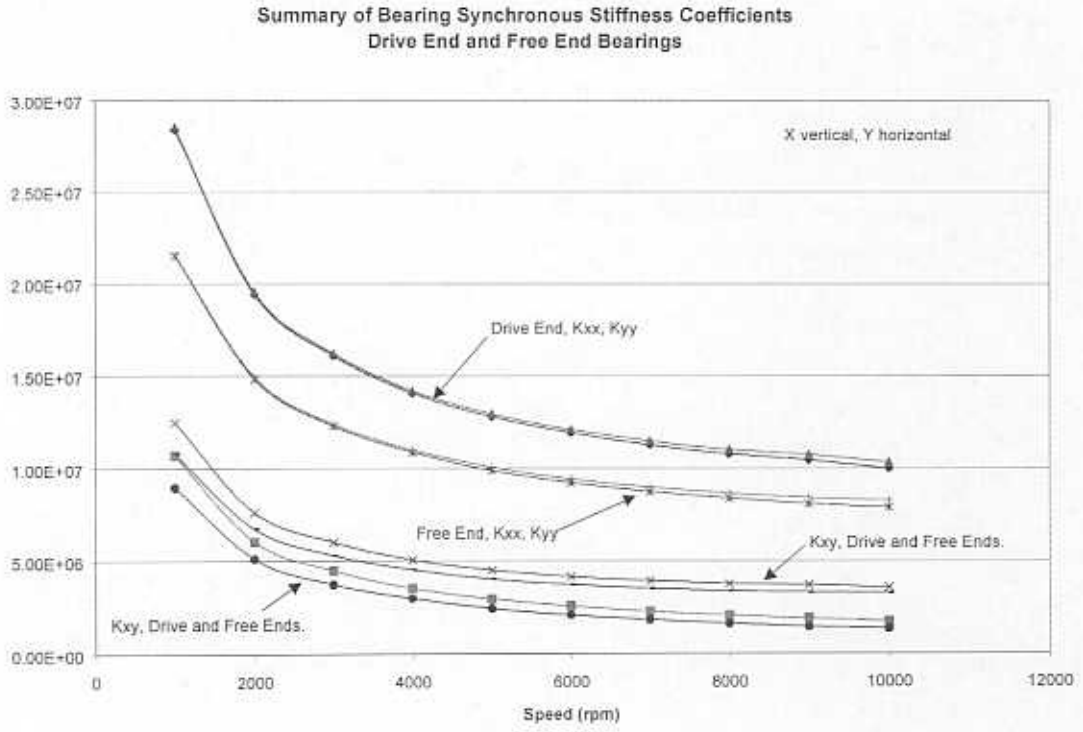

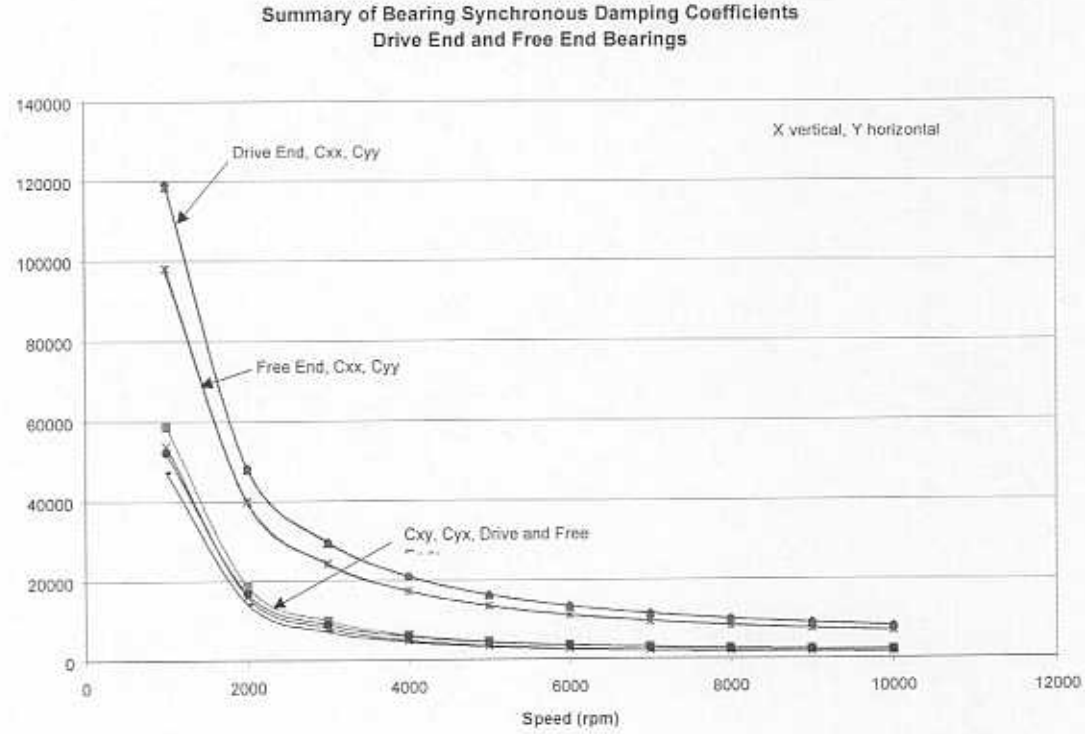

Figure 21. Predicted synchronous stiffness and damping force coefficients of flexure pivot tilting pad journal bearings at drive and free ends (X: vertical, Y: horizontal).

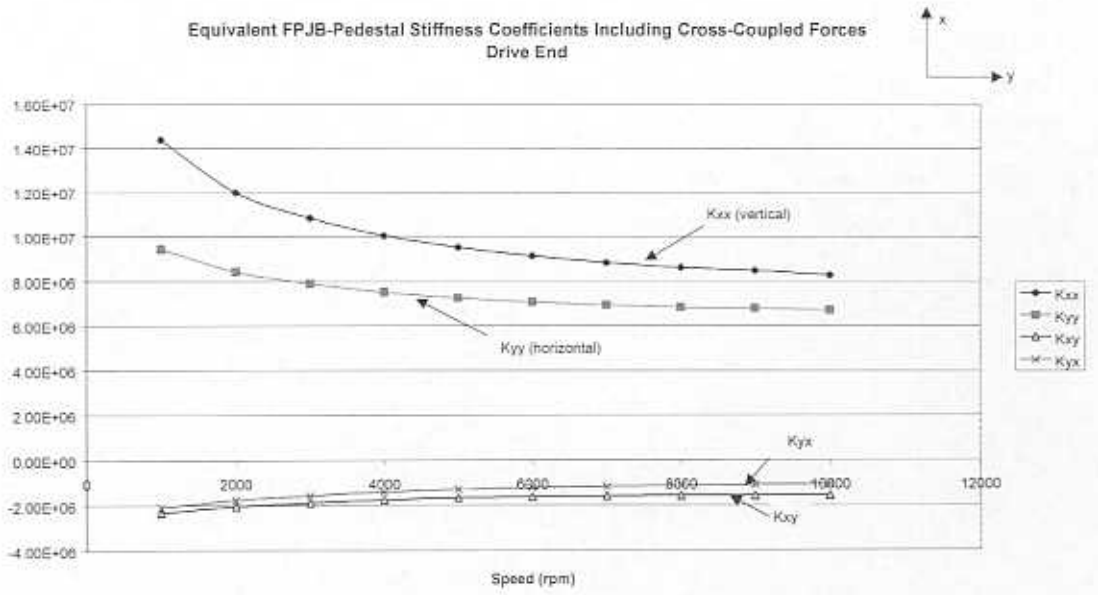

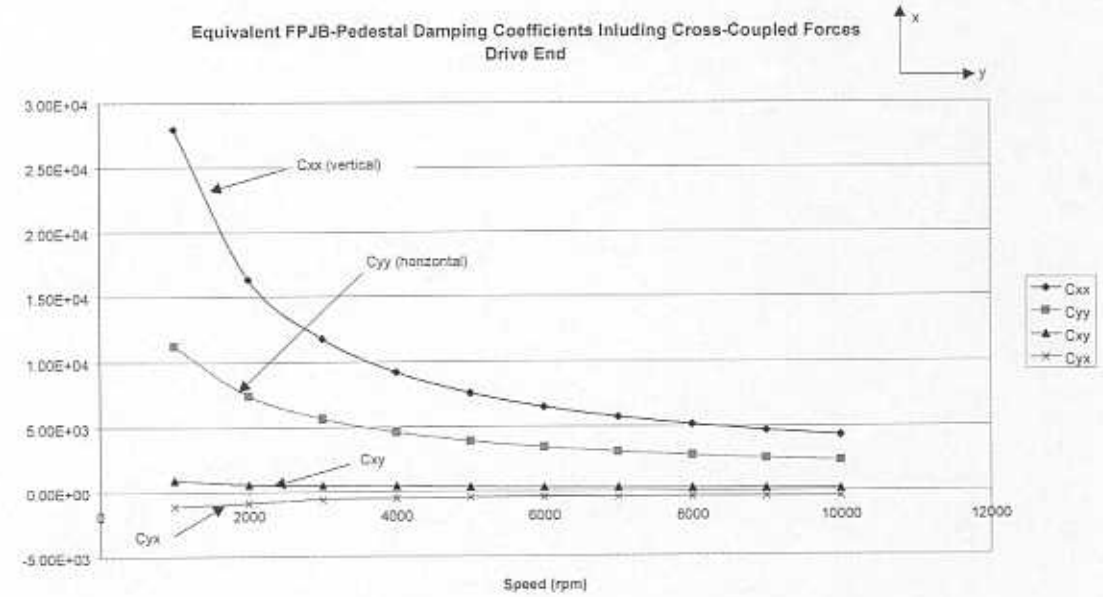

Figure 22. (a) Equivalent force coefficients for series *FPJB* and pedestal support. Drive end support.

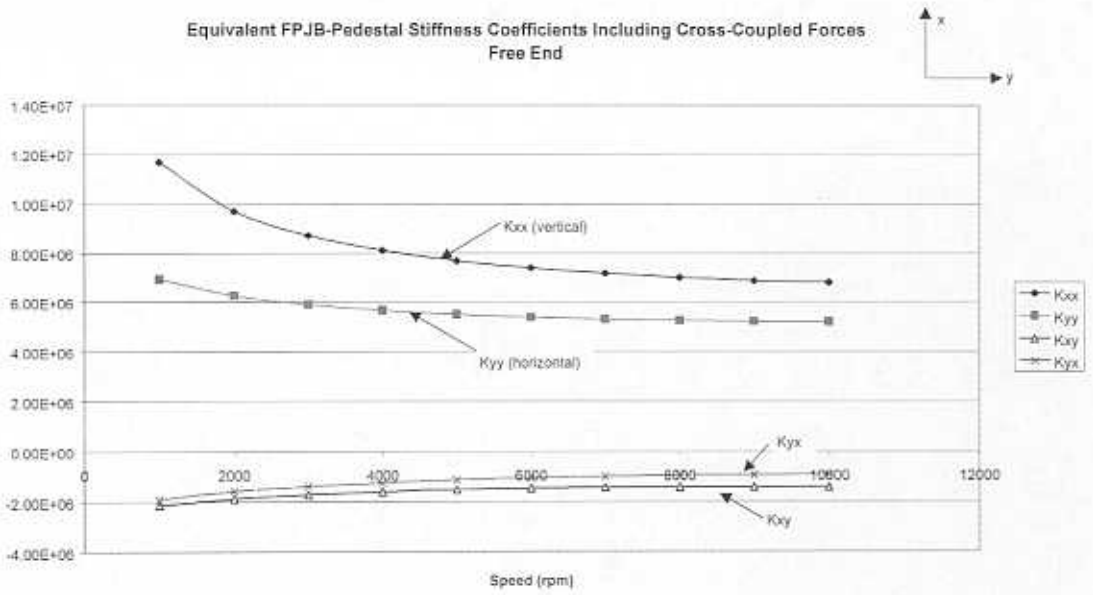

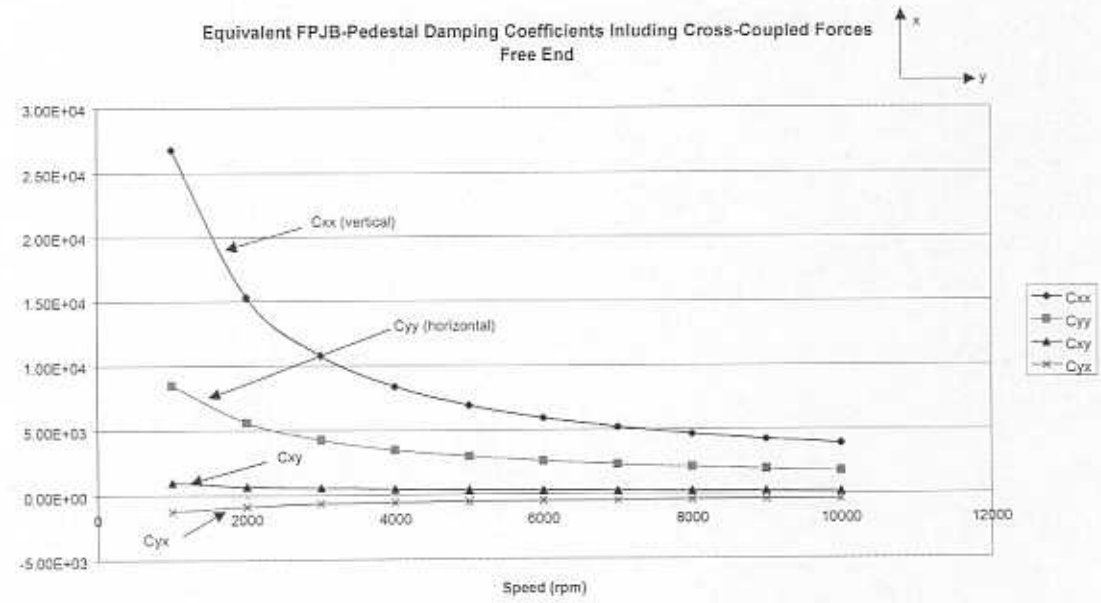

Figure 22. (b) Equivalent force coefficients for series *FPJB* and pedestal support. Free end support.

Figure 23 shows the predicted and experimental synchronous response of the test rotor at its midspan for a mass imbalance of 5 grams. The predictions for motion in the vertical direction match very well the experimental measurements over the entire speed range. However, the correlation between predictions and measurements in the horizontal is less compelling. Note that the imbalance response in the horizontal plane does not even show the passage through the critical speed.

In general, the measurements evidence a (vertical) rotor response nearly proportional to the imbalance displacement (u), even though the recorded amplitudes of motion are of large magnitude with respect to the bearing clearance.

An equivalent system damping ratio (ξ) for vertical motions can be estimated from the peak response at the critical speed. The simple relationship is used,

$$\xi^2 = \frac{-1 \pm \sqrt{1 + 1/Q^2}}{2} \tag{2}$$

where Q is the system amplification factor given by the slope of the line relating peak amplitudes at the critical speed and the imbalance distance (u). From the results given in Figure 15, $Q=5.5$ and the damping ratio is

$$\xi_{V,a} = 0.179 \tag{3a}$$

The subindex (a) denotes the configuration of the rotor mounted on tilting pad bearings and locked *SFDs*. Note that damping ratios in excess of 50% would be obtained in the horizontal direction since the response does not show a peak value. The simple analysis based on peak responses follows the assumption of rotor rigidity and plain flexible damped supports. The equivalent system damping and stiffness coefficients for motions in the vertical direction are just,

$$C_{V,a} = \xi_{V,a}\, C_{crit} = \xi_{V,a}\, 2\, (K_{V,a}\, M)^{1/2} = 2\, \xi_{V,a}\, M\, \omega_{n,a} = 9{,}782 \text{ kNs/m} \tag{3b}$$

$$K_{V,a} = M\, (\omega_{n,a})^2 = 16.48 \text{ MN/m} = 94.2 \text{ Klb/in} \tag{3c}$$

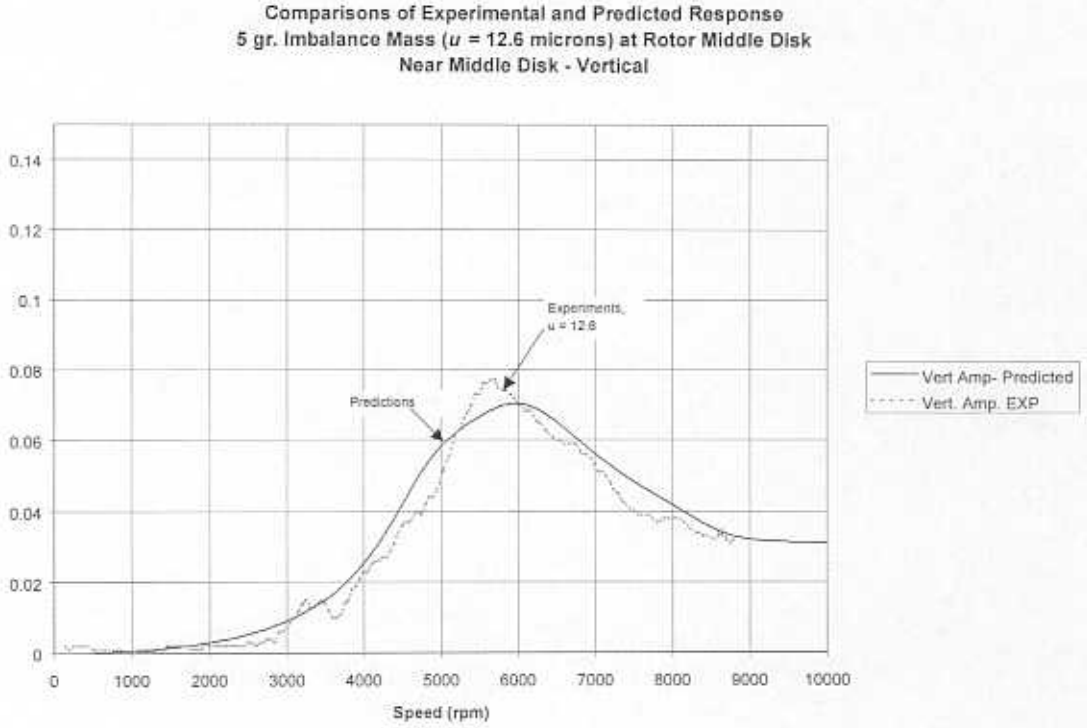

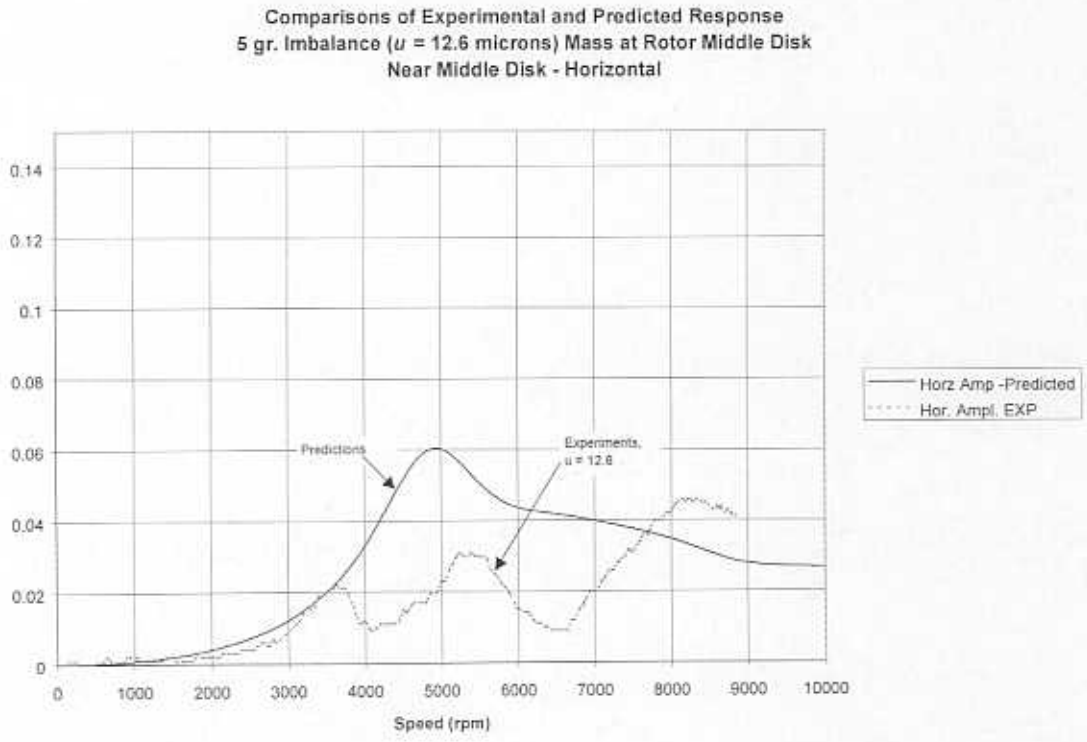

Figure 23. Comparison of predicted and measured synchronous response for 5 gram imbalance (u=12.6 microns). Measurements at rotor midspan.

where M=45.3 kg is the rotor mass, and $\omega_{n,a}$= 603.2 rad/s (5,760 cpm) corresponds with the average measured natural frequency, and which is very close (almost identical) to the predicted natural frequency. Note that the values of damping ratio and natural frequency correlate well with the predictions shown in Table 7, i.e $\xi_{V,a}$ =0.203

Results of imbalance response for rotor supported on series tilting pad bearings and integral dampers

Imbalance response experiments were conducted to assess the dynamic behavior of the rotor supported on the Flexure Pivot Tilting Pad bearings in series with the Integral Squeeze Film Dampers. The integral dampers provide a flexible support that relocates the system first critical speed and allows for increased rotor orbital motions (due to larger imbalances) while reducing force transmissibility to the supports. The squeeze film lands are open to ambient in the current tests (no end seals installed).

Table 8 sums the imbalance conditions and inlet lubricant temperatures. The largest imbalance displacement *(u)* corresponds to 49 microns (18.7 grams), i.e. larger than twice the largest value tested with the *FPJBs* alone. Figure 24 depicts the compensated rotor synchronous response at midspan for increasing imbalances. Similar measurements were recorded at the free and drive ends and not shown for brevity. Note that the amplitudes of rotor vibration in the vertical and horizontal directions are nearly identical while crossing the new lower critical speed at approximately 2,700 rpm. Note also the appearance of a peak response in the vertical direction at about 4,500 rpm, and ascribed to a resonance of the bearing pedestals. No subsynchronous vibrations were ever observed in any of the experiments.

Table 9 presents the peak-peak amplitudes of rotor response at the first critical speed and estimates of the average amplitude and standard deviation in the three planes of measurement. Figure 25 shows the average critical speeds (vertical and horizontal) versus the imbalance displacement. Note the remarkable reduction in critical speed of almost 10% for the largest imbalance condition tested. Figure 26 shows the average peak amplitudes at the critical speed versus the imbalance distance. Note that the rotor amplitudes of motion are proportional to the imbalance displacement (u), in spite that the largest rotor motions are about 70% of the damper radial clearance.

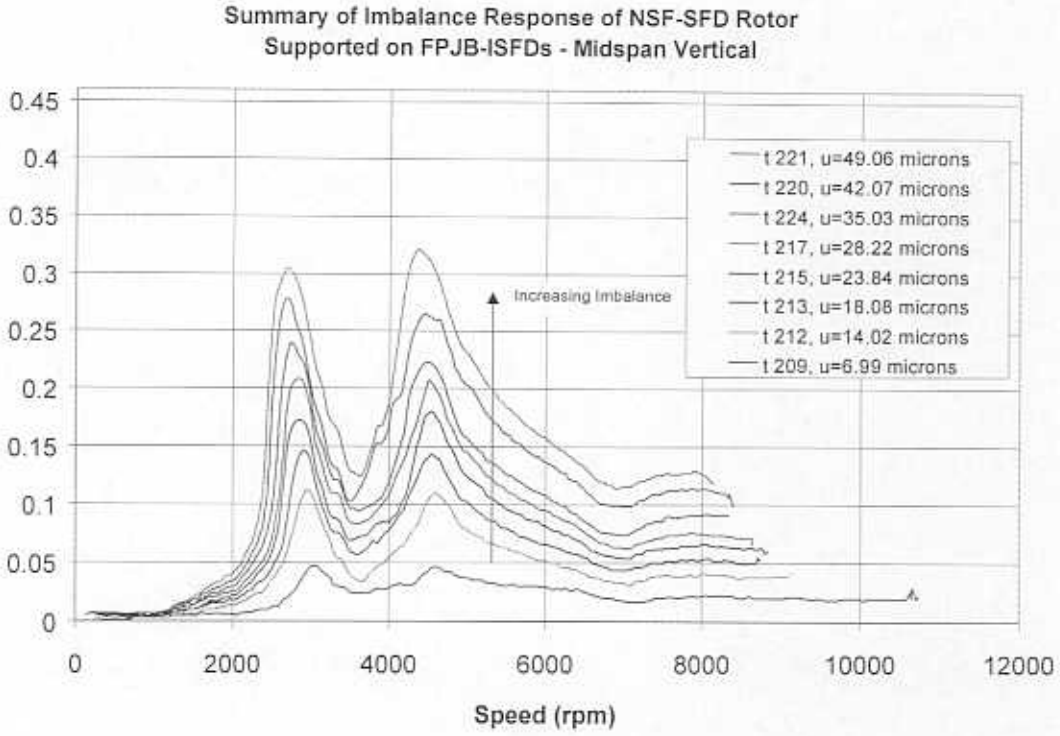

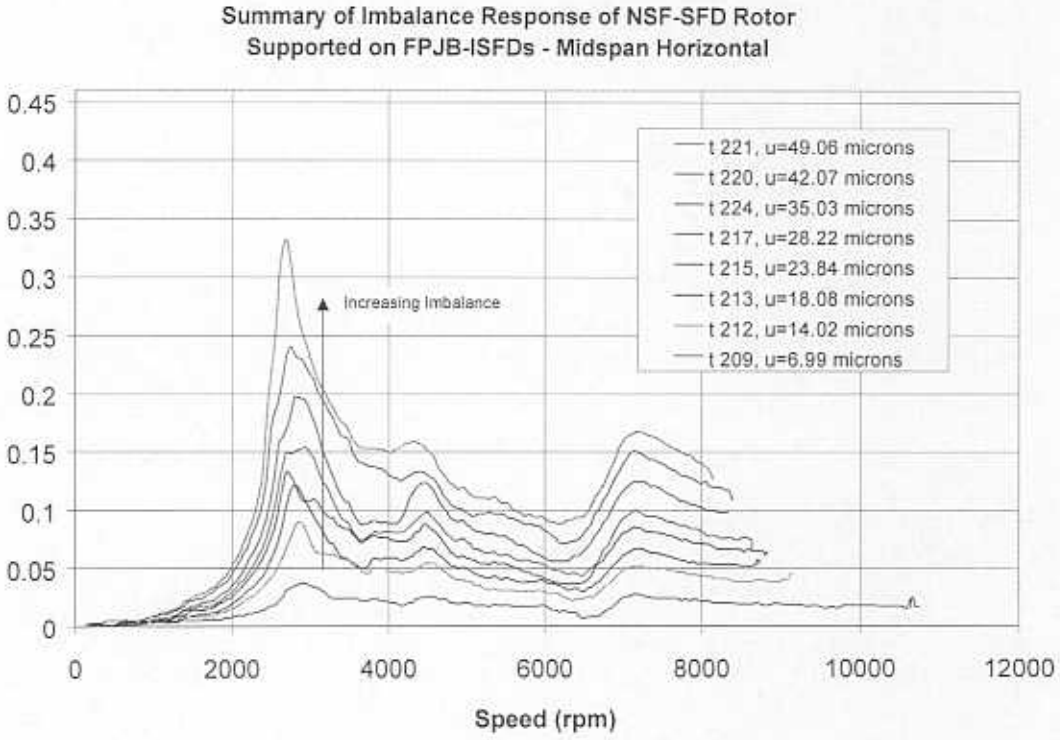

Figure 24. Imbalance response of rotor supported on series *FPJB-ISFDs*. Measurement at rotor midspan (vertical and horizontal). Dampers active.

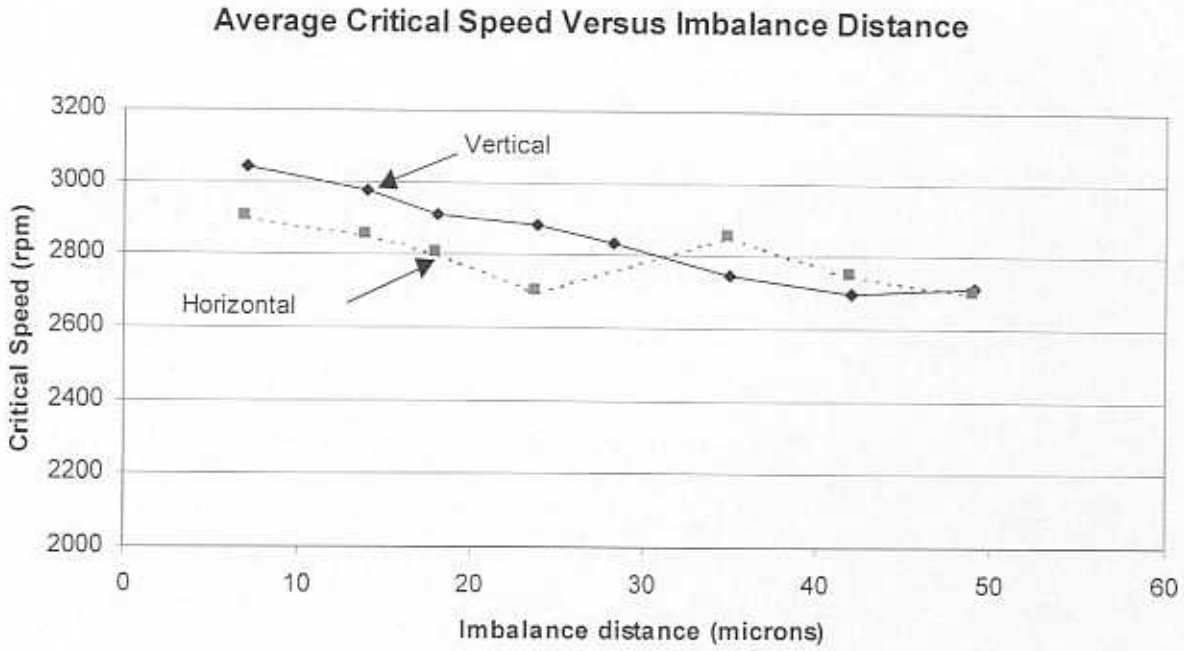

Figure 25. Measured first critical speed versus imbalance distance for tests on rotor supported on series *FPJB-ISFDs*.

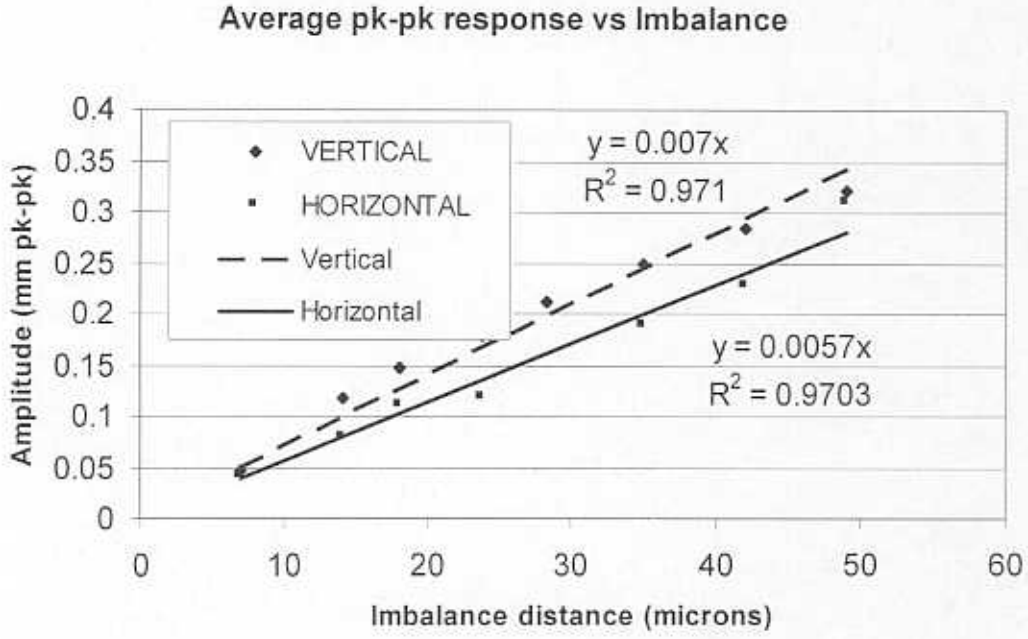

Figure 26. Average peak-peak rotor response at first critical speed versus imbalance distance for rotor supported on *FPJB-ISFDS*. Vertical direction and horizontal planes.

The equivalent system damping ratios (ξ) are estimated from the peak responses using equation (2). Recall that the simple analysis has grounds on the rigidity of the rotor, as the experimental results demonstrate. The amplification factors Q from the linear regressions given in Figure 26 are equal to 3.5 and 2.85 in the vertical and horizontal directions. Thus, the corresponding damping ratios are:

$$\xi_{V,b} = 0.141,\ \xi_{H,b} = 0.173 \qquad (4a)$$

where the subindex (b) denotes the configuration of rotor mounted on tilting pad bearings and active integral dampers.

Recall that the average damping ratios determined in prior experiments for the rotor supported on integral dampers and ball bearings are $\xi_{V,c} = 0.137$ and $\xi_{H,c} = 0.106$ (De Santiago et al., 1997). Thus, the present test configuration shows a marked increase in system damping of about 60% for motions in the horizontal direction. The increase in damping ratios for motions in the vertical direction is more modest (only 2.9%).

The corresponding equivalent damping and stiffness coefficients, $C_b = 2\,\xi\,(K_b\,M)^{1/2}$ and $K_b = M\,(\omega_{n,b})^2$, in the vertical and horizontal directions are equal to

$$C_{V,b} = 4.28 \text{ kNs/m},\ K_{V,b} = 5.09 \text{ MN/m} \qquad (4b)$$

$$C_{H,b} = 4.92 \text{ kNs/m},\ K_{H,b} = 4.46 \text{ MN/m} \qquad (4c)$$

where M=45.3 kg is the rotor mass, and $\omega_{n,b}$= 335 and 314 rad/s (3,200 and 3,000 rpm) are the predicted[1] natural frequencies (critical speeds) in the vertical and horizontal directions, respectively.

Figure 27 presents dimensionless amplitudes of response of the rotor supported on the series *FPJBs* and *ISFDs* at midspan for two different levels of imbalance distance (u). The corresponding imbalance distance is used to produce dimensionless rotor responses as in the tests with *FPJBs* and locked dampers. The dimensionless responses are not exactly proportional to the imbalance displacement as was the case for the test results of the rotor on *FPJBs* alone (see Figure 16). Nonetheless, the overall response of the rotor supported on the series support does show a linear trend (see Figure 26 for peak amplitudes at the critical speeds) with increased tolerance to large imbalances.

[1] The experimental critical speeds decrease from 3,000 to 2,700 rpm and 2,900 to 2,700 rpm as the imbalance increases (see Figure 25).

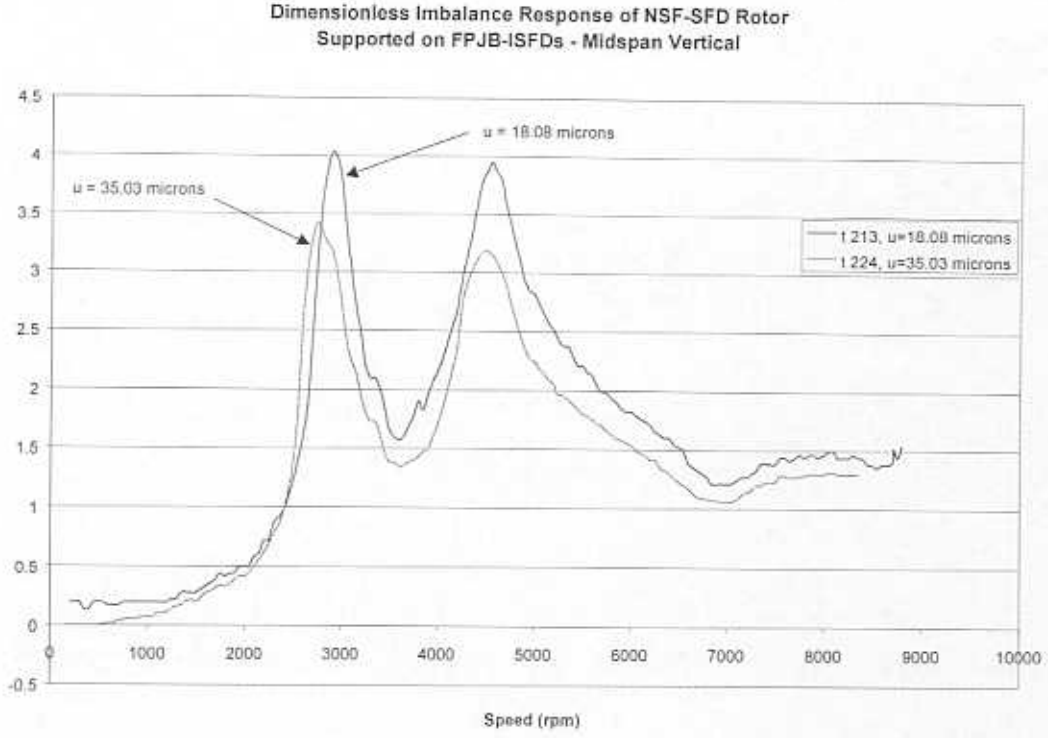

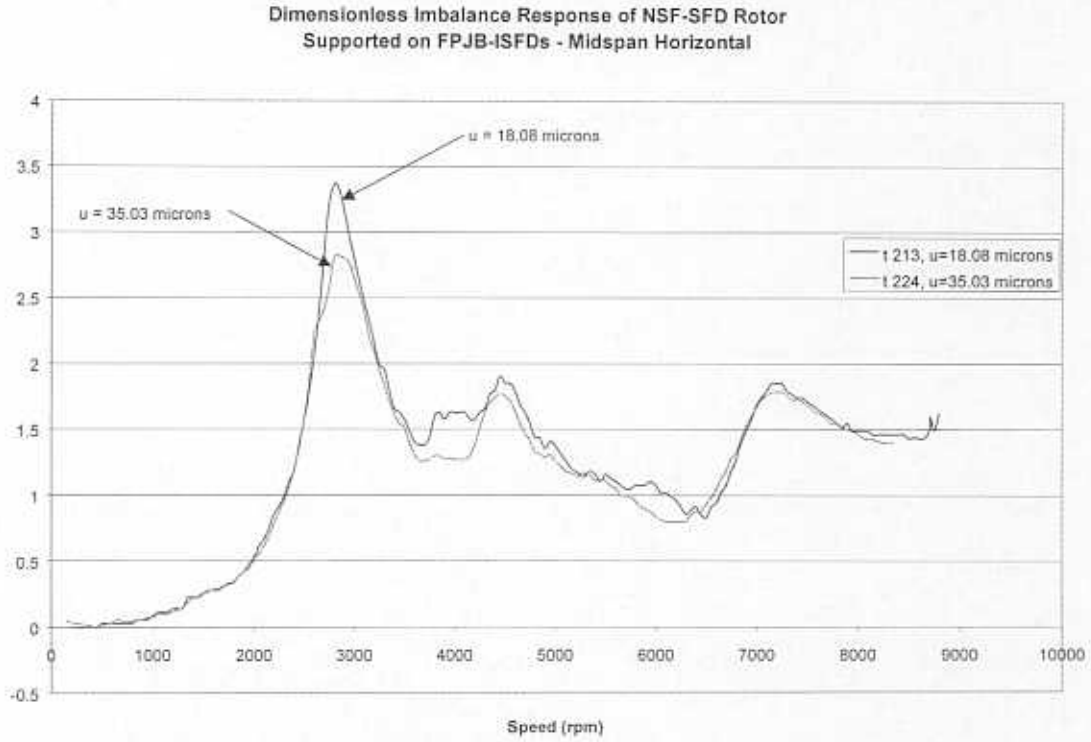

Figure 27. Dimensionless imbalance response of rotor supported on series *FPJBs* and *ISFDs*. Measurements at rotor midspan.

Predictions of imbalance response for rotor supported on series tilting pad bearings and integral dampers

Table 10 shows the average system damping coefficients determined from the peak amplitude of response at the critical speeds for the rotor supported on the *FPJBs* (locked dampers) and the rotor supported on the series tilting pad bearings and integral dampers. The table includes the system damping coefficients determined in prior measurements for the rotor supported on ball bearings and open-ended *ISFDs* under similar operating conditions of lubricant temperature (73-75°F) and with the same oil type (De Santiago et al, 1997). Values of the system damping coefficients from the impact response experiments, Figure 13, at the same temperature as the imbalance response measurements are also given in the Table 10.

The identified system damping coefficients from imbalance responses are larger than the damping coefficients derived from the impact tests at the corresponding lubricant viscosities (28% average increment in the vertical direction, and 106% average increment in the horizontal direction). The larger values show the viscous action of the lubricant film in the tilting pad bearings. Note also that the horizontal damping coefficient from imbalance tests is now larger than the vertical damping coefficient, as opposed to the identified damping from impact tests.

Figure 28 shows the predicted equivalent force coefficients for the series *FPJBs* and *ISFDs*. The *ISFD* stiffness is the result of the combination of the *ISFD* structural stiffness and that of the flexible pedestal (see Table 6). The damping coefficients of the open-ended *ISFDs* are the values identified from previous imbalance measurements with rolling element bearings, as given in Table 10. The coefficients for the tilting pad bearings were predicted using the computational program *HydroTRCM* ©. The equivalent force coefficients show very low cross-coupled effects arising from the tilting pad bearing. As expected, the contribution of the integral damper flexibility is evident in the equivalent support stiffness, which is greatly reduced as compared to the stiffness of the bearing and pedestals only (see Figure 21).

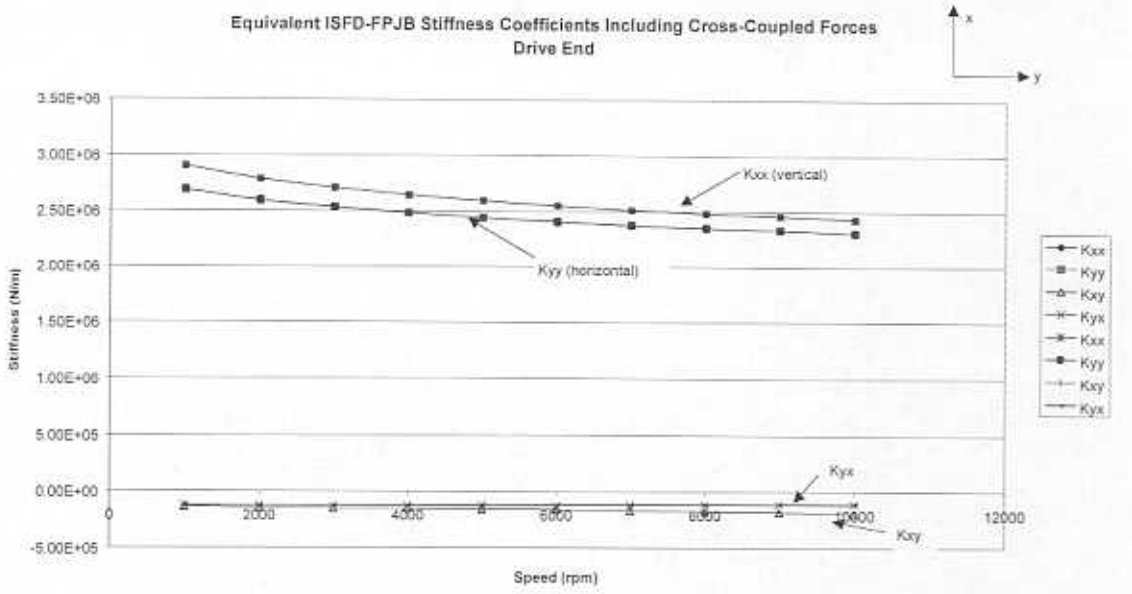

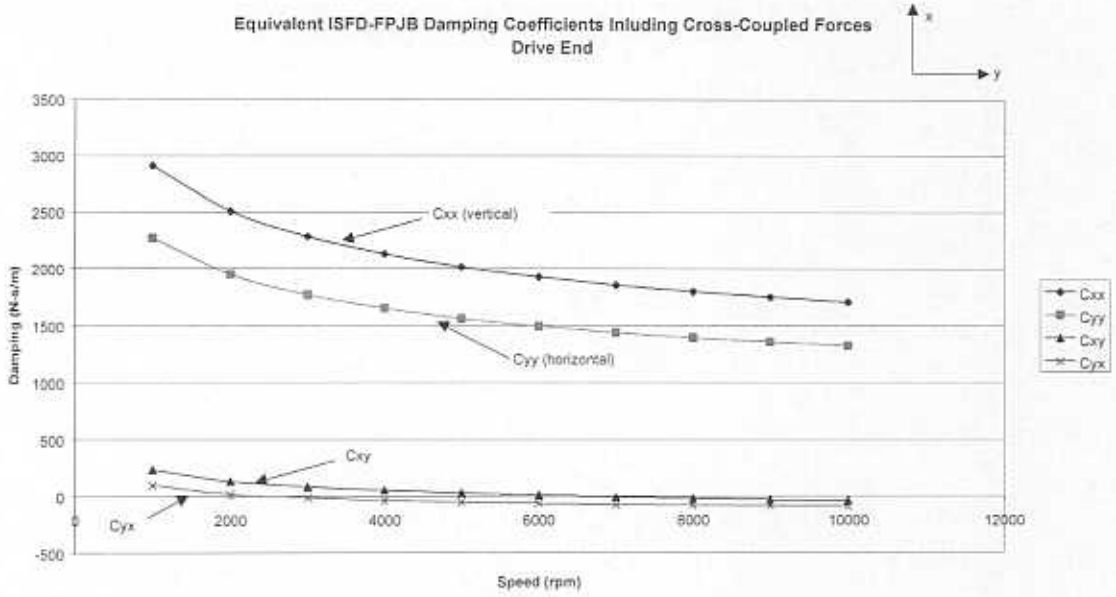

Figure 28a. Predicted equivalent stiffness and damping synchronous force coefficients for tilting pad bearings and integral dampers, including supports flexibility. Drive end support.

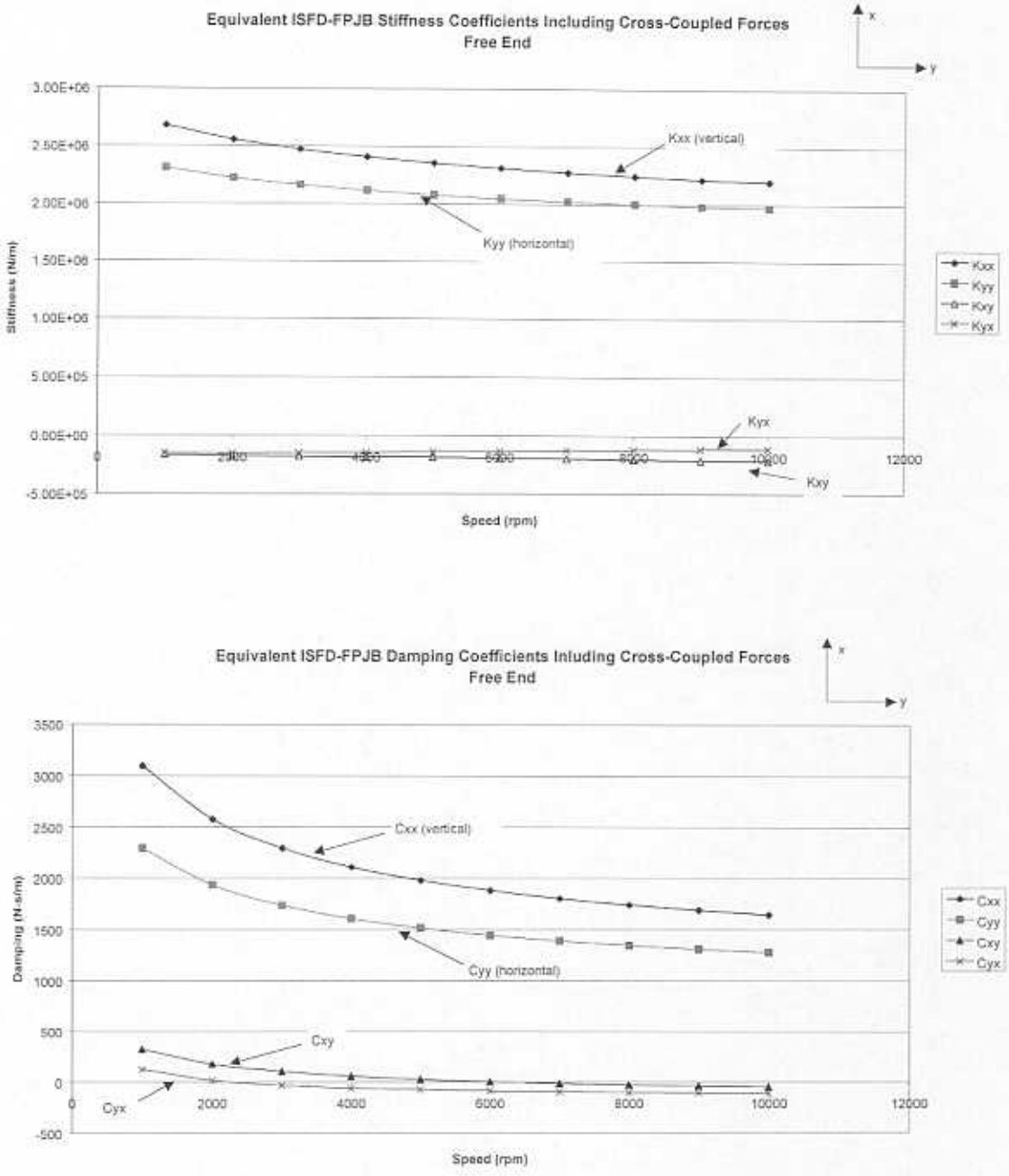

Figure 28b. Predicted equivalent stiffness and damping synchronous force coefficients for tilting pad bearings and integral dampers, including supports flexibility. Free end support.

Table 11 presents the calculated system critical speeds and damping ratios for rotor speeds below 10,000 rpm. All predicted modes of vibration are well damped within the range of test speeds. The predicted damping ratios for the cylindrical mode of vibration compare relatively well with the values derived from the measurements ($\xi_{V,b} = 0.141$, $\xi_{H,b} = 0.173$). The differences are 5% and 26% in the vertical and horizontal directions, respectively.

Figure 29 shows a comparison of the experimental and predicted synchronous rotor response for the largest imbalance (18.6 gram), u=0.049 mm. Note that the test response in the vertical directions shows the resonance of the support, not well accounted for in the predictive model. Predicted amplitudes of response at the critical speed are in general closer to the experimental measurements in the horizontal direction. Improved comparisons are apparent for lower imbalances, but not included for brevity.

Figure 30 shows the measured response of the test rotor for different bearing support configurations corresponding to tilting pad bearings (*FPJBs)* with active and locked integral dampers (*ISFDs),* and ball bearings with active integral *SFDs.* De Santiago et al (1997) studied this last configuration earlier. The figure depicts the rotor response for very similar imbalances and lubricant temperatures (viscosities), yet not identical for the cases shown. Note the remarkable effect of the tilting pad bearings on the rotor response with respect to that obtained from ball bearings, i.e. the viscous action of the fluid film bearing is obvious. The response for tilting pad bearings with locked dampers shows low amplitudes of vibration but can tolerate imbalances not large enough to cause rotor motions not exceeding the tilting pad bearing clearances. On the other hand, the combined tilting pad bearing and integral damper support can accept much greater imbalances with a well damped response. Note that the flexibility of the integral damper support reduces (by design) the critical speed of the rotor supported on tilting pad bearings and attenuates the transmitted forces to ground.

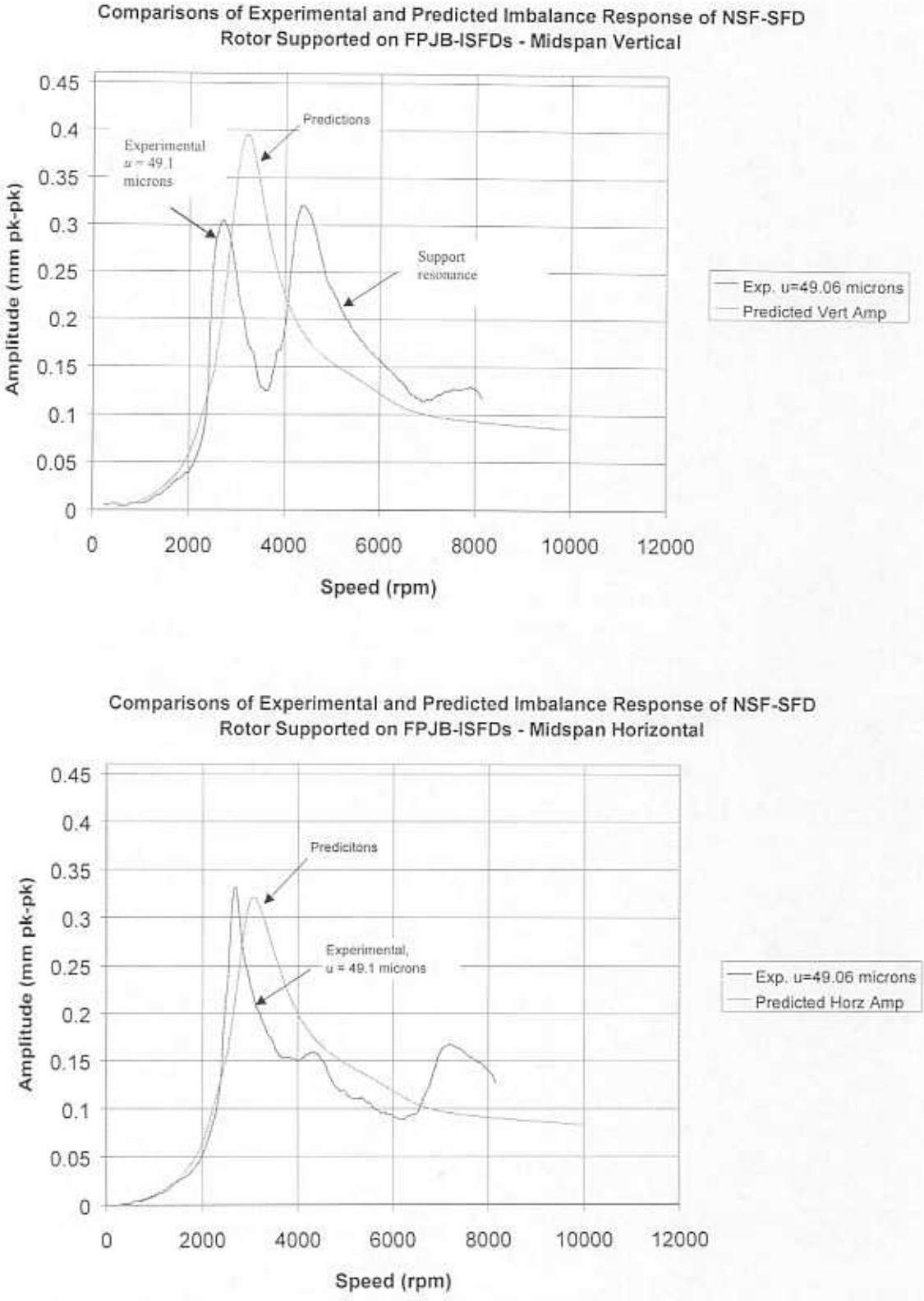

Figure 29. Comparison of predicted and measured synchronous response for 18.6 gram imbalance (u=49 microns). Measurements at rotor midspan (Integral dampers active).

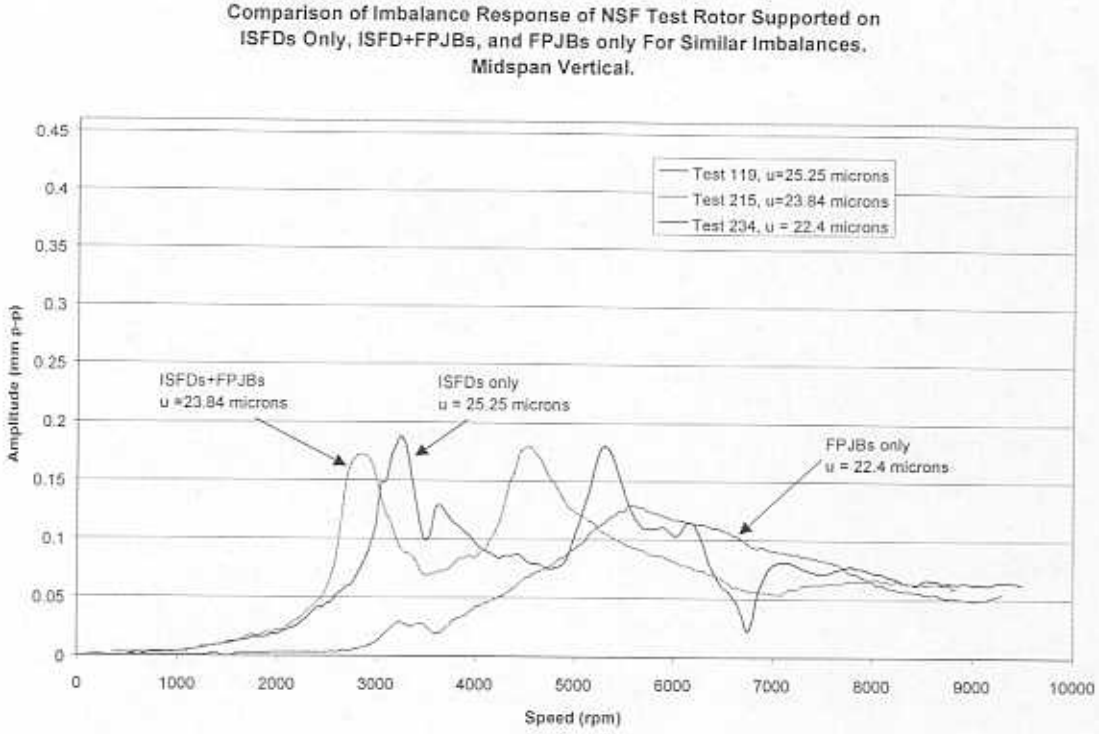

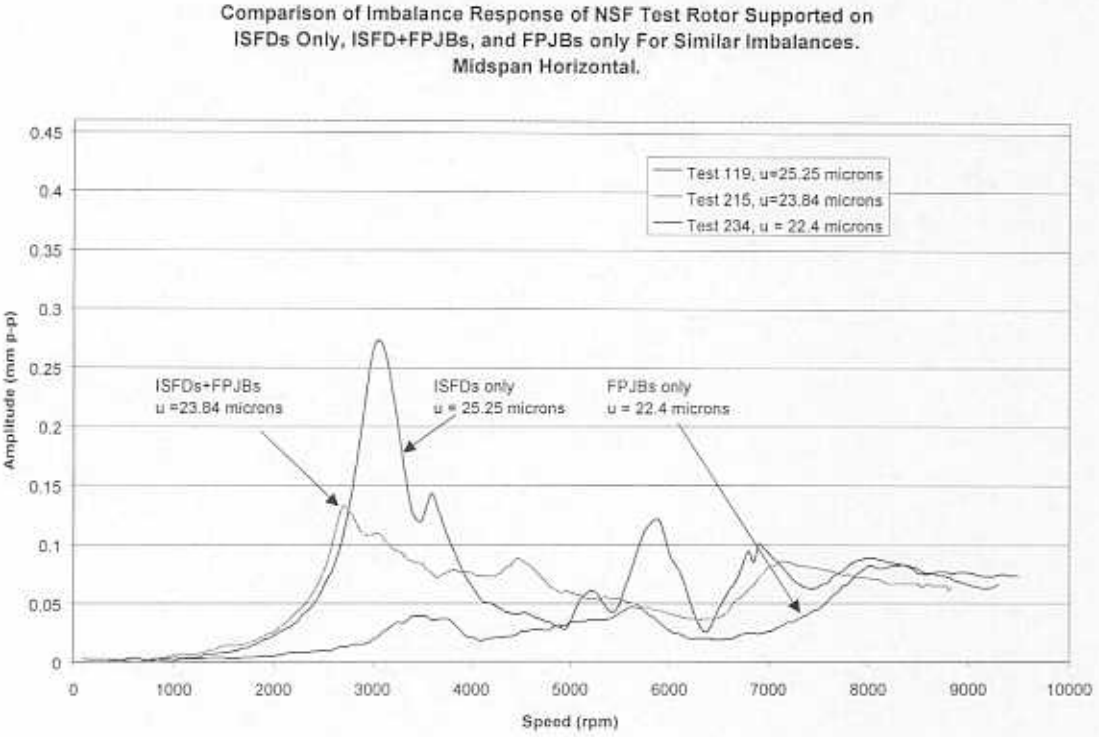

Figure 30. Imbalance response of rotor supported on different bearing support configurations: tilting pad bearings with active and inactive dampers, and ball bearings with active dampers. Measurements at midspan.

CLOSURE

The present investigation details measurements of the imbalance response of a three disk massive rotor supported on flexure pivot tilting pad bearings in series with integral squeeze film dampers. The experiments aimed to identify the effectiveness of the series support on the relocation of system critical speeds and optimum damping coefficients to ensure a safe rotor response with an increased tolerance to disk imbalance.

Coast-down experiments from 10 krpm were conducted for increasing levels of disk imbalance. The measurements show the rotor center line moves in a nearly vertical direction, thus evidencing little cross coupled effects in the flexure pivot bearings. System damping coefficients are identified from the peak amplitude of rotor response (Q-factor) while traversing cylindrical mode critical speeds (~ 5,700 rpm for locked *SFDs* and 3,200 rpm for active *SFDs*). The tests performed with locked (inactive) and active *ISFDs* demonstrate the effectiveness of the flexible damped support in reducing the system critical speed and improving the overall rotor response with reduced transmitted forces to ground. The *ISFDs* allow the rotor to operate safely with values of imbalance twice as large as the maximum sustained by the rotor supported on tilting pad bearings only.

The support configuration of flexure pivot bearings and integral squeeze film dampers shows many advantages over the common ball bearing-*SFD* arrangement. These are namely, easiness of installation and retrofit (split elements), reduced number of parts and weight, and as demonstrated by the measurements, much larger viscous damping action with increased tolerance to disk imbalances. The engineered structural webs on the integral dampers also allow the accurate location of rotor-bearing system critical speeds.

Comparisons of the experimental and predicted responses establish in a global sense the validity of the analytical models for prediction of force coefficients in tilting pad bearings. Predicted system damping ratios compare well with those estimated from the peak amplitude responses. Critical speeds are also favorably predicted. However, further experimental effort is needed to develop parameter identification techniques that will allow the estimation of the bearing and damper force coefficients over frequency ranges of interest.

REFERENCES

Childs, D., 1993, "Turbomachinery Rotordynamics," John Wiley & Sons Pubs, N.Y.

Dede, M. M., M. Dogan, and R.Holmes, 1985, "The Damping Capacity of a Sealed Squeeze Film Bearing," Transactions of the ASME, *Journal of Tribology*, Vol. 107, July, pp. 411-418.

De Santiago, O., Oliveras, J., and San Andrés, L., 1997, "Imbalance Response of a Rotor Supported on Integral Open Ends *SFDs*," Turbomachinery Research Consortium Annual Report, Texas A&M University, TRC-*SFD*-2-97, April.

De Santiago, O., and San Andrés, L., 1998, "Imbalance Response of Rotor Supported on Sealed Integral Dampers," Turbomachinery Research Consortium Annual Report, Texas A&M University, TRC-*SFD*-1-98, May.

De Santiago, O., and San Andrés, L., 1999 "Design of a Series Tilting Pad Bearing and Squeeze Film Damper for NSF-TRC Rotordynamics Test Rig and Analysis for Optimum Damping at Bearing Supports," Turbomachinery Research Consortium Annual Report, Texas A&M University, TRC-*SFD*-1-99, May.

San Andrés, L., 1996, "Turbulent Flow, Flexure-Pivot Hybrid Bearings for Cryogenic Applications," ASME Journal of Tribology, Vol. 118, 1, pp. 190-200.

Zeidan, F., 1995, "Application of Squeeze Film Dampers", *Turbomachinery International*, Vol. 11, September/October, pp. 50-53.

TABLES

Table 1. Measured viscosity of ISO VG 10 lubricant.(*)

Specific gravity = 0.845

Temperature ° C (°F)	Viscosity (cP)
15.4 (59.7)	22.53
17.3 (63.1)	21.60
21.6 (70.1)	17.50
25.0 (77.0)	14.75
30.5 (86.9)	11.68
34.0 (93.2)	10.53
37.0 (98.6)	9.45
40.0 (104.0)	8.40
43.0 (109.4)	7.20
46.8 (116.2)	7.00
50.2 (122.4)	6.00

*Voghs law renders the relationship between the lubricant temperature and viscosity as $\mu = \mu_{ref} e^{\alpha(T-T_{ref})}$, where μ_{ref} = 17.03, T_{ref} = 22.3, and α =-0.038 for the current oil..

Table 2. Flexure pivot tilting pad bearing main dimensions and operating conditions.

4 pads (70°)

Bearing nominal diameter:	30.15 mm	1.187 in
Bearing axial length:	22.9 mm	0.902 in
Pad radial clearance:	0.127 mm ± 0.005 mm	0.0050 in ± 0.00013 in
Pad preload: 0.405 (r_p)	0.0508 mm	2 mils
Pivot offset:	0.50	
Bearing radial clearance:	0.076 mm	3 mils
Pad rotational stiffness:	40 N-m/rad	354 lb-in/rad
Clearance on back of pads:	0.178 mm (typ)	0.007 in (typ)
Average inlet lubricant viscosity	15.76 cP	at 24.4° C (76° F)
Operating speed range:	0-10,000 rpm	
Static load between pads		
drive end bearing	247.3 N	55.53 lb (51.90 psi – specific load)
free end bearing	198.2 N	44.50 lb (41.56 psi - specific load)

Table 3. Mass imbalances for tests with rotor supported on *FPJBs* (locked dampers).

Test #	Imbalance mass	Imbalance distance u	Av. Oil Temp.
	gram	μm	°C (°F)
236	3.5	8.81	22.7 (72.9)
228	5.0	12.6	24.6 (76.4)
232	6.9	17.4	24.2 (75.7)
234	8.9	22.4	22.4 (72.3)

The imbalance distance is calculated from $u = (m\ r/M_r)$ where u is the imbalance distance, m is the imbalance mass, r = 114.3 mm (4.5 in) is the radius of the disk where the imbalance mass is attached, and M_r = 45.3 kg is the rotor mass (for the fundamental mode of vibration).

Table 4. Peak-peak amplitudes of motion at the first critical speed for rotor supported on tilting pad bearings.

Bearing diametrical clearance (between pivots) = 0.152 mm (0.006 in)

Peak-peak amplitude (mm) and critical speed (rpm) VERTICAL DIRECTION										
Test #	Imbalance distance u	Drive		Middle		Free		Average Amplitude	Standard dev.	Average critical speed
	μm	mm	rpm	mm	rpm	mm	rpm	mm	mm	rpm
236	8.81	0.062	5600	0.071	5700	0.057	5925	0.063	0.006	5742
228	12.6	0.065	5600	0.077	5700	0.064	6100	0.069	0.006	5800
232	17.4	0.094	5650	0.111	5700	0.092	5900	0.099	0.009	5750
234	22.4	0.119	5650	0.129	5600	0.102	6075	0.117	0.011	5775

Table 5. Predicted and measured free-free natural frequencies (Hz) of test rotor.

Nat. Frequency	1st	2nd	3rd	4th
Rotor only (no coupling hub)				
Experimental:	656 to 664 Hz	968 Hz	1,420 Hz	2,800 Hz
Model:	656 Hz	967 Hz	1,423 Hz	2,560 Hz
Rotor with coupling hub installed				
Experimental:	268 Hz	952 Hz	1,420 Hz	2,000 Hz
Model:	270 Hz	962 Hz	1,387 Hz	1,891 Hz

Uncertainty in measurements:
(+/-) 2 Hz, 1st and 2nd natural frequencies, (+/-) 5 Hz, 3rd and 4th natural frequencies.

Table 6. Stiffness for pedestal supports and integral dampers.
Source: De Santiago et al (1997)

		Drive end MN/m, (lb/in)	Free end MN/m (lb/in)
ISFD structural stiffness (from static measurements)	Vertical	3.66 (20,878)	3.50 (19,965)
	Horizontal	3.80 (21,677)	3.53 (20,136)
Pedestal support stiffness (from impact tests)	Vertical	30.50 (174,000)	28.20 (160,900)
	Horizontal	13.95 (79,580)	10.10 (57,600)
Equivalent support stiffness (series *ISFD* and pedestal)	Vertical	3.26 (18,600)	3.11 (17,700)
	Horizontal	2.99 (17,060)	2.62 (14,950)

Table 7. Predicted critical speeds and damping ratios of test rotor supported on *FPJBs* only.

Rotor speed (rpm)	*Natural frequencies (cpm) and Mode of vibration*							
	Cylindrical, Forward, *Horizontal*		Cylindrical, Forward, *Vertical*		Conical Backward		Conical Forward	
	Freq. (cpm)	Damping ratio	Freq. (cpm)	Damping ratio	Freq. (cpm)	Damping ratio	Freq. (cpm)	Damping ratio
4000	4791	0.194	5877	0.252	7382	0.214	9112	0.187
4500	*4750*	*0.182*	5833	0.234	7245	0.211	8876	0.180
5000	4722	0.170	5792	0.218	7108	0.208	8719	0.169
5500	4691	0.160	*5760*	*0.203*	6970	0.205	8616	0.156
6000	4663	0.149	5723	0.189	6834	0.199	8549	0.142
6500	4638	0.140	5694	0.175	*6700*	*0.193*	8508	0.129
7000	4617	0.131	5669	0.163	6592	0.187	8487	0.117
7500	4601	0.124	5646	0.154	6491	0.182	8484	0.108
8000	4590	0.119	5628	0.148	6403	0.179	8496	0.101
8500	4583	0.116	5612	0.145	6325	0.178	*8518*	*0.096*

Table 8. Mass imbalances for tests with rotor supported on series *FPJB-ISFDs* (dampers active).

Test #	Imbalance mass	Imbalance distance *u*	Av. Oil Temp.
	gram	μm	°C (°F)
209	2.67	6.99	24.8 (76.7)
212	5.33	14.02	23.5 (74.4)
213	6.88	18.08	23.2 (73.8)
215	9.07	23.84	24.0 (75.2)
217	10.8	28.32	23.5 (74.3)
224	13.3	35.03	24.9 (76.9)
220	15.9	42.07	25.8 (78.4)
221	18.7	49.06	25.9 (78.6)

Table 9. Peak-peak amplitudes of motion at the first critical speed for rotor supported on series *FPJB-ISFDs*.

FPJB diametrical clearance (between pivots) = 0.152 mm (0.006 in)
ISFD diametrical clearance = 0.457 mm (0.018 in)

VERTICAL DIRECTION Max pk-pk amplitude (mm) and Critical speed (rpm)										
Test #	Imbalance distance *u*	Drive		Middle		Free		Average Amplitude	Standard dev.	Average critical speed
	μm	mm	rpm	mm	rpm	mm	rpm	mm	mm	rpm
209	6.99	0.051	3050	0.042	3025	0.047	3050	0.047	0.004	3041
212	14.02	0.125	2975	0.11	2950	0.116	3000	0.117	0.006	2975
213	18.08	0.157	2900	0.14	2900	0.144	2925	0.147	0.007	2908
215	23.84	0.195	2900	0.169	2850	0.174	2900	0.179	0.011	2883
217	28.32	0.228	2800	0.201	2850	0.207	2850	0.212	0.012	2833
224	35.03	0.271	2750	0.24	2750	0.236	2750	0.249	0.016	2750
220	42.07	0.305	2700	0.274	2700	0.274	2700	0.284	0.015	2700
221	49.06	0.332	2700	0.332	2700	0.303	2750	0.322	0.014	2716

Table 9. Peak-peak amplitudes of motion at the first critical speed for rotor supported on series *FPJB-ISFDs* (continued).

HORIZONTAL DIRECTION Max pk-pk amplitude (mm) and Critical speed (rpm)										
Test #	Imbalance distance *u*	Drive		Middle		Free		Average Amplitude	Standard dev.	Average critical speed
	μm	mm	rpm	mm	rpm	mm	rpm	mm	mm	rpm
209	6.99	0.038	2850	0.041	2950	0.043	2900	0.041	0.002	2900
212	14.02	0.076	2850	0.09	2850	0.071	2850	0.079	0.008	2850
213	18.08	0.107	2800	0.123	2800	0.098	2800	0.109	0.010	2800
215	23.84	0.119	2700	0.134	2700	0.098	2700	0.117	0.015	2700
217	28.32									
224	35.03	0.177	2850	0.197	2800	0.189	2900	0.188	0.008	2850
220	42.07	0.231	2750	0.242	2750	0.209	2750	0.227	0.014	2750
221	49.06	0.318	2700	0.318	2700	0.291	2700	0.309	0.013	2700

Table 10. Average system damping coefficients for the different bearing-damper support configurations.

As determined from imbalance response measurements and impact tests

	Vertical	Horizontal
Rotor on *FPJBs* only (locked *ISFDs*)	$9.78^{\pm 0.90}$ kNs/m (55.8 lb.s/in)	NA (**)
Rotor on *FPJBs* and active *ISFDs*	$4.28^{\pm 0.21}$ kNs/m (24.4 lb.s/in)	$4.92^{\pm 0.25}$ kNs/m (28.1 lb.s/in)
Impact response measurements	~3.35 kNs/m at 75 °F (16.0 cPoise)	~2.38 kNs/m at 77 °F (15.4 cP)
Rotor on *ISFDs* only (ball bearings) (*)	$4.36^{\pm 0.13}$ kNs/m (24.9 lb.s/in)	$3.14^{\pm 0.10}$ kN-s/m (17.9 lb.s/in)

(*) Prior measurements conducted by De Santiago et al. (1997)

(**) Measured rotor response did not show critical speed excitation.

Table 11. Predicted critical speeds and damping ratios of test rotor supported on *FPJBs* in series with *ISFDs*.

Rotor speed (rpm)	*Natural frequencies (cpm) and Mode of vibration*							
	Cylindrical, Forward, *Horizontal*		Cylindrical, Forward, *Vertical*		Conical Backward		Conical Forward	
	Freq. (cpm)	Damping ratio	Freq. (cpm)	Damping ratio	Freq. (cpm)	Damping ratio	Freq. (cpm)	Damping ratio
2500	3010	0.132	3216	0.139	4452	0.211	5370	0.197
3000	*2991*	0.127	*3199*	0.134	4340	0.204	5444	0.186
3500	2974	0.122	3183	0.130	4232	0.198	5520	0.177
4000	2959	0.118	3168	0.127	*4129*	0.194	5599	0.169
4500	2945	0.115	3153	0.124	4029	0.190	5680	0.162
5000	2932	0.112	3140	0.122	3932	0.187	5763	0.156
5500	2920	0.109	3127	0.120	3838	0.184	5847	0.150
6000	2909	0.107	3115	0.118	3747	0.181	*5933*	0.144

Experimental system damping ratios: $\xi_{V,b} = 0.141$, $\xi_{H,b} = 0.173$
Average critical speeds: Vertical 3,000-2,700 rpm, Horizontal: 2,900-2,700 rpm (Figure 25)